August 2018

Hydrophobic Self-Cleaning Coatings for Sustainable Infrastructure

Evgeniya Alexandrova
University of Wisconsin-Milwaukee

HYDROPHOBIC SELF-CLEANING COATINGS FOR SUSTAINABLE INFRASTRUCTURE

by

Evgeniya Alexandrova

A Thesis Submitted in

Partial Fulfillment of the

Requirements for the Degree of

Master of Science

in Engineering

at

The University of Wisconsin-Milwaukee

August 2018

ABSTRACT

HYDROPHOBIC SELF-CLEANING COATINGS FOR SUSTAINABLE INFRASTRUCTURE

by

Evgeniya Alexandrova

The University of Wisconsin-Milwaukee, 2018
Under the Supervision of Professor Konstantin Sobolev

Durable two-layer hydrophobic coatings with photocatalytic properties demonstrated a good decomposition of NO_x up to 23 %. The first layer of the coating is based on the application of durable titanium phosphate structures. The hydrophobic properties of the coating with a water contact angle of 114° were achieved by the application of water-based siloxane emulsion on the surface of the first layer. Conducted research has demonstrated that the use of hydrophobic coating in comparison with reference TiO_2-phosphate can slightly reduce the efficiency for the decomposition of NO_x by 8 %; however, this feature can be considered as an acceptable trade-off between the potential improvement of durability of the coating and photocatalytic performance. The formation of layers with very small, around 100 μm, thickness allows to avoid the formation of cracks observed for thicker coatings and contributes to better adhesion of the coating to the surface of substrate material.

TABLE OF CONTENTS

LIST OF FIGURES

LIST OF TABLES

LIST OF ABBREVIATIONS

A	Ampere
a.u	Arbitrary Units
CA	Contact Angle
CO	Carbon Monoxide
COF	Coefficient of Friction
CLSM	Confocal Laser Scanning Microscope
eV	Electron Volt
K.	Degrees of Kelvin
MPa	Mega Pascal
N	Newton
ppb	Parts per Billion
ppm	Parts per Million
PVA	Polyvinyl Alcohol
Rpm	Revolutions per Minute
SEM	Scanning Electron Microscope
UV	Ultra Violet
VOC	Volatile Organic Compounds
XRD	X-Ray Diffraction

ACKNOWLEDGEMENTS

I would like to thank my advisor, Professor Konstantin Sobolev, whose guidance has been critical to successful research projects. I also would like to thank Dr. Marina Kozhukhova for the assistance and valuable advices during the research. Especial thanks to Sridhar Lanka for his huge help with tribological and confocal tests. Additional thanks to Dr. Habib Tabatabai, Dr. Michael Nosonovsky, and Dr. Benjamin Church for serving on my thesis committee and offering valuable feedback.

1. Introduction

1.1. Photocatalytic concrete

The alarming rise in anthropogenic air pollutions, evident in urban areas, induced the need to create new photocatalytic materials with self-cleaning properties which can combat the car exhaust fumes and other forms of harmful pollutants in the air. By application of building materials with photocatalytic response, engineers can decrease the impact of these pollutions on human health and the environment [6]. Imparting photocatalytic properties to the facades, roads and other structures without any adverse effect to their original properties including color is commonly realized by applying a thin layer of coating material based on titanium dioxide (TiO_2). Optionally, this coating layer can use cement paste to adhere the active components to the surface of structure and TiO_2 can be incorporated as a component of concrete [6, 34]. The main component of photocatalytic coatings, TiO_2 is a common white pigment that is harmless, inexpensive and currently is widely used in paint, plastics, cosmetics, sunscreen, toothpaste, and other products [26].

There are three polymorph modifications of titanium dioxide: anatase, brookite, and rutile. Rutile is the most commonly occurring type of TiO_2, which has chemically resistant properties and also high refractive index. Anatase converts to rutile after heating at about 915 °C [16, 36]. Anatase has almost the same properties as rutile with regards to its density and hardness. Both anatase and rutile have tetragonal crystalline structures, but anatase has octahedrons that share four edges forming the four-fold axis. Crystal structures of anatase and rutile are demonstrated in Figure 1.1. The X-ray diffractograms of rutile titanium dioxide and anatase titanium dioxide are reported in Figure 1.2. Anatase is not advisable to use it outdoor applications because it has a lower water

absorption rate than rutile [36]. Still, anatase is also used as a white pigment in paints, paper, and ceramics.

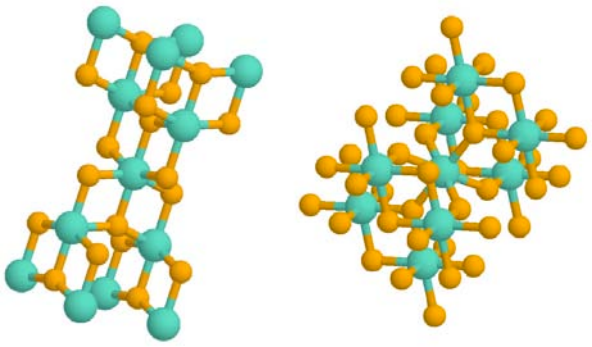

Figure 1.1. Extended crystal structure of anatase (left) and rutile (right) [30]

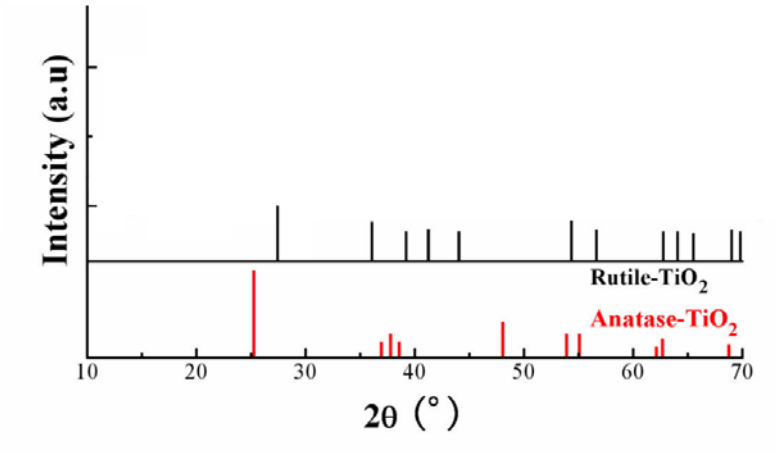

Figure 1.2. X-ray diffractograms of rutile and anatase TiO_2 [33]

The application of TiO_2 as a component of concrete can require the use of a relatively large amount of TiO_2 (up to 15 % of cement replacement) [31]. However, the presence of photocatalyst is only required at the surface of the material. Paint applications can suffer the photocatalytic and UV decomposition of polymer films resulting in a release of TiO_2 nanoparticles on the surface, easy removal, and associated health issues.

In this regard, a little effort has been made in optimizing the application procedure for photocatalysts. The application procedure should be cost effective and should not result in inferior physical, chemical and mechanical characteristics of concrete or another substrate. The application of the sprayable photocatalytic coating on the surface of concrete, capable of chemically bonding with the substrate, can be a more effective way to increase the photocatalytic and self-cleaning properties of structure achieved at fewer amounts of titanium dioxide [34]. Importantly, such coating should be resistant to erosion and abrasion, and nanoparticles of TiO_2 should not be washed out by water [13]. The outdoor environments with high wind speeds and humidity may affect the performance of coatings based on titanium dioxide particles. A new coating combining hydrophobic properties along with photocatalytic response can become a new generation of materials offering the better performance of TiO_2-based products [13].

Definition of photocatalysis

Photocatalysis is defined as a process of acceleration of a chemical reaction in the presence of a catalyst, and this method was successfully applied for the decomposition of harmful substances in air and water [32]. The photoreaction is a charge separation of electrons and creation of electron-hole pairs on the photocatalytic surface commonly occurring under the ultraviolet irradiation [9]. These electrons generate free hydroxyl radicals and superoxide anions which can react with air pollutants, decomposing these into small amounts of relatively harmless solid compounds. The primary catalytic component, the anatase polymorph of titanium dioxide (TiO_2), is a commonly used white pigment. The mechanism of photocatalysis is reported in Figure 1.3.

1. TiO_2 + UV-light → e^- + $hole^+$
2. e^- + $hole^+$ → TiO_2 + Heat or
3. $hole^+$ + OH^- →OH· & e^- + O_2 → O_2^-·
4. R· + NO_x → Intermediates → NO_3+H_2O

Figure 1.3. The schematics of photocatalytic decomposition of air pollutants [32]

According to the van Driel and Kooyman [32], if one of the steps resulting in radical formation is prevented, the photocatalytic reaction will stop. This happens, for example, when the surface of titanium dioxide nanoparticles is covered with an inorganic surface coating. In this case, the coating creates the barrier between the catalytic molecules and organic compounds in the air acting as an ultraviolet light absorber. Therefore, the main problem is to attach the particles of TiO_2 to the surface, which preserves the ability to generate free radicals.

The free radicals help to break down the nitrogen oxides (NO_x), volatile organic compounds (VOC's), carbon monoxide (CO) and organic pollutants which are generated in the air from industrial smog, power generated car exhaust fumes and the other outcomes of human activities and to oxidize these into inorganic compounds such as carbon dioxide, nitrates, sulfates, etc [23].

Photocatalytic concrete

Many field and laboratory experiments proved that the application of photocatalytic titanium dioxide in pavements, cladding elements, architectural precast panels, exterior plaster, windows, stucco, noise barriers for roads and other types of structures significantly reduces the concentration of harmful gases in the air approximately by 45 %, and up to 60 % in some applications, helping to keep the original color of structure [10]. Also, photocatalytic materials reflect much of the sun's

heat, reducing the air temperature on the structural surfaces and the amount of smog in urban environments during the summer.

Many types of building materials with photocatalytic properties have been produced over the last twenty years. The application of nano-particles includes the improved paint coatings and cement, improved insulation materials with a porosity of the order of 10 to 100 nm, polymer-based floor coatings, nano-filters to purify water and asphalt blends with the oxidation resistance [7].

Photocatalytic coatings have been applied on glass windows to decompose dirt particles and to provide infrared and ultraviolet screening on windows. Architectural precast panels were manufactured, using white cement with TiO_2 and demonstrated the aesthetic characteristics over the time along with the effective removal of pollutants. White cement with self-cleaning properties has been used for the construction of modernistic “Dives in Misericordia” church in Rome [26]. New photocatalytic cements and TiO_2 products can be used to produce concrete that saves costs on maintenance and, at the same time, cleans the environment. Photocatalytic concrete was used as a self-cleaning material in many civil engineering and architectural projects in Japan [4].

An example of the application of titanium dioxide in photocatalytic concrete is Baton Rouge, Louisiana where the ¼ mile of a concrete roadway was covered with a photocatalytic coating, with a purpose to demonstrate the ability of TiO_2 to decompose and reduce the amount of nitrogen oxides in the air. The concentrations of NO_x were measured, and the results of initial monitoring demonstrated that the developed coating was effective in reducing NO_x.

Researchers proved that many factors affect the effectiveness of photocatalytic materials, such as solar radiation, light intensity, relative humidity and wind direction and speed (Dylla et al., 2012) [31, 7]. In 2002, photocatalytic TX Active® mortar was

tested for photocatalytic properties. A section of the asphalt surface in Via Morandi in Segrate (province of Milan) was covered with TX Active®. This road has a traffic flow of around 1,000 vehicles/hour. Tests proved the degradation and reduction of nitrogen oxides by 60 %. These projects have demonstrated that a concrete road made of photocatalytic concrete can reduce the NO_x levels by 20 to 80 %, depending on atmospheric conditions. Following this success, new highway using of TiO_2 was constructed in St. Louis, MO in 2011 [7].

Types of photocatalysts

Some semiconductors can act as effective photocatalysts. The surface energy and chemisorption properties of photocatalysts play key roles in the transfer of electrons and in determining the vulnerability of the photocatalyst toward photo-corrosion. In general, higher surface energy yields a higher catalytic activity. For this reason, metal oxide semiconductors such as TiO_2, ZnO, Fe_2O_3, CdS, and ZnS are considered to be the most effective photocatalysts due to wide band gap energy and photo-corrosion resistance [2, 9]. Table 1.1 provides the band gap energies at a corresponding wavelength for well-known photocatalysts.

Titanium dioxide has been most commonly used as the "ideal" photocatalyst due to its ability to decompose organic pollutants achieving complete mineralization, its high reactivity, chemical stability, reduced toxicity and lower costs [2]. Photocatalytic efficiency of different types of TiO_2 depends on the surface and structural properties which include the surface area, crystal composition, porosity, particle size distribution and band gap energy.

Table 1.1. Band gap energies of various photocatalysts at relevant wavelengths [2]

Semiconductor	Band gap energy (eV)	Wavelength (nm)
TiO_2 (rutile)	3.0	413
TiO_2(anatase)	3.2	388
ZnO	3.2	388
ZnS	3.6	335
CdS	2.4	516
Fe_2O_3	2.3	539

Factors affecting the degradation performance

The concentration of titanium dioxide particles on the surface affects the overall photocatalytic reaction rate, which is directly proportional to the amount of TiO_2 deposited on the surface. However, when the concentration of titanium dioxide is above a certain level (saturation stage), the light photon adsorption coefficient decreases and this can lead to light screening effect, to the reduction of the surface area exposed to the irradiation and thus to the reduction of the photocatalytic efficiency [2].

Particle size is an important factor to be considered in the photocatalytic degradation process because there is a direct relationship between the surface area of the photocatalyst and the reduction of organic compounds. Different forms of titanium dioxide have been developed to achieve the desired characteristics of the photocatalyst, including commonly used P25, PC500, UV100 and TTP products. The efficiency of these photocatalysts in the degradation of organic compounds has been reported by Degussa to be in the order of

P25 > UV100 > PC500 > TTP [2].

In general, the increase of reaction temperature results in the increased photocatalytic activity, however the reaction temperature higher than 80^{o}C leads to the recombination of charge carriers and reduces the adsorption of organic compounds on

the surface of the photocatalyst. Preferable temperature range for effective photo-mineralization of organic content lies between 20 – 80 $^{\circ}$C [2].

Some studies have proved the dependency of the photocatalytic reaction rate on the concentration of contaminants. High concentration of pollutants reduces the photonic efficiency of the photocatalyst. Also, the chemical structure of an organic compound influences the degradation performance of the photocatalyst. For instance, the decomposition of 4-chlorophenol requires extended irradiation [2, 20].

The influence of humidity on the photocatalytic reaction rate was well investigated. Researchers proved that the increase in humidity could negatively affect the photocatalytic degradation under UV light irradiation. Engel investigated the influence of different humilities (between 6 % and 90 %) on the photocatalytic reaction rate of TiO_2 [12]. The experiment demonstrated that the conversion of NO_x decreased with increasing humidity. It was found that for the best photocatalytic effect the optimum air humidity is in the range of 20-40 %.

The conversion of NO compounds was found to be strongly affected by the UV irradiance. The increase of UV irradiance results in increasing photocatalytic reaction rates. According to Engel, the degradation of NO compounds in the presence of UV(A) irradiation increases with increasing the irradiance in a non-linear manner [12]. Figure 1.4 demonstrates the conversion of NO vs. UV photon flux during the photocatalytic oxidation of NO in the presence of P25.

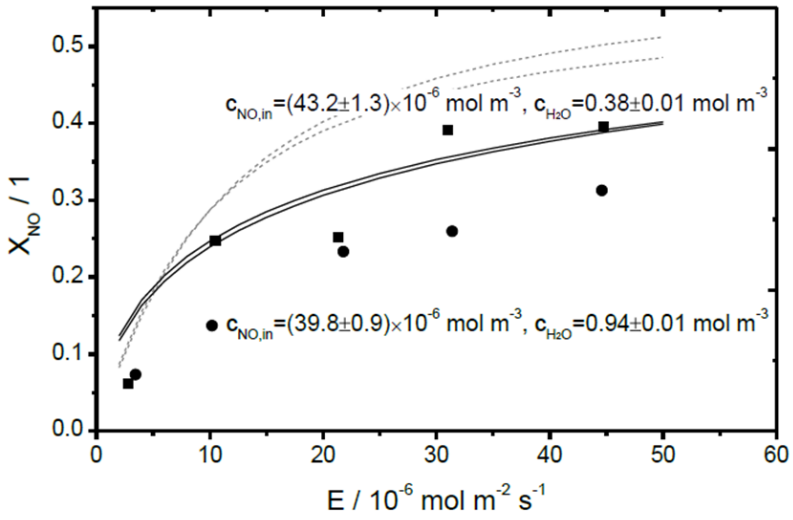

Figure 1.4. Fractional conversion of NO vs. UV(A) photon flux during the photocatalytic oxidation of NO in the presence of UV(A) irradiated P25 samples [12]

1.2. Chemistry of phosphate cement

A binder is any substance that draws and holds other materials and compounds together to form a chemically and mechanically cohesive composite, by adhesion or cohesion. Binders are classified as organic (including polymers, glues, and bitumens), and inorganic such as lime, gypsum, portland cement and based on liquid glass (geopolymers, alkali-activated compounds based on sodium or potassium silicates).

Inorganic (mineral) binders are finely powdered substances, which when mixed with water (sometimes with salt), form a plastic moldable compound that hardens and binds together different filler and aggregate components. Organic binders are mixtures of high-molecular-weight hydrocarbons, viscous or liquid materials that are processed for application by thermal, ultraviolet radiation, or organic cross-linking agent treatment [37].

Inorganic binders can be classified by the type of hardening process as hydraulic (hydraulic lime, portland cement), non-hydraulic with air hardening mechanism

(magnesium oxide, gypsum), autoclave (which harden at 170 to 300 °C and pressure of up to 20 atm to comprise CSH composites), alkali- and acid-activated [37].

The type of initial components determines the specific properties of synthesized cement composites, which, in particular, include the phosphate cement. For example, phosphate hardening occurs when special chemical compounds, usually oxides, react with phosphoric acid. The main chemical process that initiates the hardening of phosphate cement systems is the acid-base interaction of liquid protonated environment with solids. The basis for the synthesis of binders and materials is any reaction of acid-base interaction in heterogeneous dispersed systems of solid-liquid type.

In such systems, development of binding properties changes for different chemical characteristics of the base. The decrease of the ionic potential of the cation in the oxide as far as the decrease of the electronic work function causes an increase in basic properties of the oxide. In this case, the chemical activity of the oxide in acid increases and so phosphate systems harden under normal conditions without heating and mechanochemical activation. The acceleration of setting and hardening processes occurs as the ion potential of the cation decreases in the groups with a uniform electron structure and, conversely, as the ion potential increases, this process slows down [40].

A necessary condition for the developing of binding properties in phosphate cement systems is the proportionality of the intensity of the main chemical process with the processes of structure formation. The excess activity of components interaction is related to the concentrated heat release in the system, and, when this process becomes autocatalytic, it leads to the destructive phenomena with the mass critically warming up and crumbling, decomposing the initially formed structure.

There are some techniques to overcome the excessive interaction activity among the components of phosphate cement:

1. Cooling of the initial components and intensive heat transfer from the mixing reactor. These techniques allow working with highly reactive systems containing cations such as Pb^{+2}, Zn^{+2}, Mg^{+2} [40].

2. The passivation of the initial solid component. The material from which the original powder is produced is subjected to heat treatment at high temperatures. Thus, the seal of material and the reduction of the reaction activity occur. This technique is especially effective for the systems which contain oxides of cadmium, zinc, magnesium.

3. A common way of passivating the solid component is shielding of particles by surface-active substances or by diluting by inert powders, such as finely ground silica, wollastonite or fly ash [40, 5, 19].

4. The modification of the solution is based on the correction of the functional composition of the liquid component. The most common method is the preliminary neutralization of acid (cationic modification) until the transition convents the acid solvent to salt. Thus, the solvent phase for zinc phosphate or silicate cement is orthophosphoric acid, previously neutralized with oxides of aluminum, magnesium, or zinc.

The main approach to increase the activity of chemical interaction is by heating. In some cases, for example in the system of Cr_2O_3 + H_3PO_4, a similar result can be achieved by using methods of mechanochemical activation applied to powder components [40].

Properties of phosphate cement

The practical characteristics of phosphate cement have a wide range depending on the type of components and proportions used. The hardening of magnesium phosphate cement is based on the synthesis of the double magnesium ammonium

phosphate $NH_4MgPO_4 \cdot 6H_2O$ and magnesium phosphate $Mg_3(PO_4)_2 \cdot 4H_2O$. After one day of hardening under normal conditions (at room temperature and atmospheric pressure) the compressive strength can achieve up to 150 MPa [40]. Zinc phosphate cement, a combination of modified zinc oxide powder and partially neutralized orthophosphoric acid, demonstrates the highest flexural strength of up to 10 MPa after 24 hours of hardening [1]. Fast-hardening magnesium ammonium phosphate cement is a mixture of ammonium phosphates and magnesium oxide. Being mixed with water, after 1 hour this cement demonstrates the strength of up to 14 MPa [40, 27].

The strength of up to 50 MPa after 4 hours of hardening is gained by wollastonite phosphate cement, which is a combination of ground wollastonite and partially neutralized acid [40]. By 28 days of hardening, the strength of about 250 MPa is achieved by the system, represented by ferrites of zinc and copper [40]. The same level of compressive strength (up to 250 MPa) is attained by the systems processed at high (up to 1,200 °C) temperatures. This applies to materials based on fused magnesia.

When water-containing binder systems are heated, the physical and constitutional water is removed. In hydration formed systems, this process causes the destructive phenomenon, which leads to a significant (up to 90 %) loss of strength, initially gained as a result of hardening. In the case of phosphate cement, thermal dehydration is usually combined with the processes of polycondensation and polymerization of the structure-forming compounds, which favorably affects the strength.

The properties of compounds formed as a result of hardening of phosphate cement, in many cases, allow these compounds to be attributed to materials with high thermal stability. Phosphate cement systems can be used at high and even ultrahigh (up to 2,000 °C) temperatures. For example, zirconium phosphate cement, which is a combination of zirconium dioxide powder with solutions of aluminum phosphates, is

suitable for the service at up to 2,000 °C, and magnesium phosphate, which uses pure magnesium oxide and zirconium phosphate solution, up to 1,700 °C [40, 25].

As materials with different thermophysical characteristics can be used as a powder component of phosphate cement, both heat-conducting and heat-insulating phosphate cement can be obtained using this approach.

Some phosphate cement based products have the electrical resistance of up to 1 kOm. The combination of titanium nitride (TiN) and chromium metal powders with orthophosphoric acid gives an excellent conductive cement. Monolithic materials obtained by mixing ferrite mineral powders with acid phosphate solutions have a good magnetic permeability [40, 29].

1.3. Properties of titanium phosphate cement

Titanium phosphate is obtained by the reaction of titanium dioxide with orthophosphoric acid at high temperatures. To determine the optimal concentrations of titanium phosphate compounds, it is necessary to establish the optimal concentration of phosphoric acid. Table 1.2 provides the data gained during the heat treatment of cement at 573K [14].

Table 1.2. Influence of the acid concentration on cement properties [14]

Ratio TiO_2:P_2O_5 by mass	Concentration of P_2O_5, %	Acid Density, kg/m^3	Compressive Strength, MPa	Bending Strength, MPa	Water Adsorption, %
3.26 : 1	36.2	1.335	9.0	1.5	26.0
2.02 : 1	54.3	1.579	41.0	1.9	16.2
1.86 : 1	66.6	1.770	61.5	4.1	9.2
0.93 : 1	76.6	1.830	16.5	2.2	14.1

In cases where oxides are relatively inert to achieve the hardening at room temperature, hydroxides are used instead, and the resulting phosphate cement is being

heated to about 573 K. The temperature is increased slowly, and then the composite is kept for an hour at the final temperature. Titanium phosphate cement based products are produced using such a route.

The optimal P_2O_5 concentration in the mixture was reported to be about 66.6 %, and titanium dioxide content is 33.4 % [14]. The resulting cementitious matrix has a compressive strength of 61.5 MPa, bending strength of 4.1 MPa, and has a fire resistance of up to 1323-1373K. The neutral and acidic aqueous environments do not destroy the titanium phosphate cement matrix, but similarly to other phosphate compounds, it decomposes under the influence of alkalis [14].

1.4. Effect of phosphate bonds on the photocatalytic activity of titanium dioxide

The surface modification of titanium dioxide may have a significant influence on the photocatalytic process by changing the charge-transfer pathways at the TiO_2 surface. Only a few studies were focused on the effect of phosphate bonds on the photocatalytic activity of titanium dioxide. The most of earlier investigations focused primarily on the improvement of thermal stability and on the increase of acid sites and the TiO_2 surface area. Matthews reported that the incorporation of phosphate reduces the photocatalytic activity rates by 20-70 % even at millimolar concentrations [35]. However, Yu recently reported that the titanium dioxide modified by phosphate ions demonstrated a higher photocatalytic activity on oxidation of *n*-pentane in air vs. pure TiO_2. Phosphate modified titanium dioxide possessed higher photocatalytic activity because of the larger surface area and extended band gap energy. Korosi also studied titanium phosphates and found that the catalysts with a small amount of phosphate possess the increased photocatalytic activity for photodegradation of phenol and ethanol [35]. It is difficult to

determine the effect of phosphate anion on the photocatalysis, because, compared with pure titanium dioxide, modified photocatalysts exhibit an array of properties in respect of crystallite component and phase, surface area, and surface acidity. Thus, the mechanism of the improvement of photocatalytic activity using phosphates is complicated and under-investigated.

Many studies proved that for improvement of photocatalytic properties, phosphate modification should be carried out before the complete crystallization of TiO_2. According to the research data, if the phosphate anion is introduced after the crystallization of titanium dioxide, the modified catalyst holds the same crystallite phase and the surface area as the unmodified one. The effect of phosphates on the photocatalytic activity of titanium dioxide should mainly be a result of a negative electrostatic field induced by the phosphate anions on the surface of TiO_2.

Zhao investigated the electronic properties of titanium dioxide modified by phosphates [35]. For samples with phosphoric acid treated after the crystallization of TiO_2, the XRD patterns exhibited little change concerning pure TiO_2. The average crystallite size of 11.5 nm was found from broadening of the diffraction peaks. This indicates that this phosphate modification influences the crystallite size and crystalline degree of TiO_2. In cases when phosphoric acid was treated before the crystallization of TiO_2, even a small amount of phosphoric acid leads to a marked broadening of the diffraction peaks. It was reported that when the phosphoric acid ratio to the amount of titanium dioxide was equal to 0.05, the surface area was increased by 85 m^2/g, and the size of TiO_2 crystallites decreased from 11.5 to 9.0 nm. Further increase of the phosphoric acid concentration demonstrated a very little effect on the crystallite size but resulted in a significant increase in the surface area by an additional 48 m^2/g (from 167 to 215 m^2/g).

Based on these data, researchers concluded that the modification process by phosphoric acid treatment of TiO_2 could significantly reduce the growth of anatase grains and greatly increase the surface area of resulting catalysts [35]. The experimental results proved that the effect of the phosphate on the photocatalytic activity of titanium dioxide is due to the surface-bound phosphate anion, rather than to the change in the surface area (particle size) or the crystalline structure of titanium dioxide. Negatively charged phosphate anions on the surface of the photocatalyst form a negative electrostatic field on the surface of TiO_2. This can suppress the charge recombination and contribute to the separation of electrons and holes in phosphate modified titanium dioxide compared with pure TiO_2.

It was reported that phosphate modification could inhibit the absorption of most compounds and suppress their degradation [35]. On the other hand, a negative electrostatic field formed by the phosphate anions can enhance the separation of electrons and holes and force the formation of free hydroxyl radicals. As a result, the effects of phosphate anions on the photocatalytic properties depend on the type of compounds to be degraded. The phosphates greatly accelerate the degradation of compounds with weak adsorption on the TiO_2 surface or susceptive to hydroxyl radical attack due to the hydroxyl radical attack pathway [35]. However, the degradation of compounds can be significantly suppressed by the hindered adsorption of substrates for systems with strong adsorption on the pure TiO_2.

All hydrogen phosphates and phosphates of potassium, alkali, sodium, and ammonium are soluble in water; their water solutions have a pH > 7. However, the phosphates of metals in high oxidation states are insoluble in water. Titanium phosphates are also insoluble in water, but highly hydrophilic. However, hydrophobic coatings may

be applied to improve the hydrophobic properties and so boost the overall durability of titanium phosphate coatings [13].

1.5. The pathways for superhydrophobic modification

Concrete and the most of ceramic materials, like brick and tile, are hydrophilic materials, which may significantly reduce the durability of structures. Here, a super-hydrophobic coating can improve the performance of construction materials and, thus, significantly increase the durability of structures.

The change in the pore structure on concrete surface affects the migration of moisture from concrete. Water in concrete evaporates in the direction of the protective coating, which causes the expansion pressure. Thus, if concrete has an impermeable coating film having no air ventilation, the coating can experience swelling and disbondment. The coating film formed on the concrete surface should ensure ventilation so that the internal moisture is evaporated without the damage to the film [36].

To solve this problem, it is necessary to improve concrete surface pore structure by using the coating material that has the function of ventilation and, at the same time, waterproofing. Also, the surface treatment can be applied to the coated material to get the required properties. The surface treatment can be mechanical (trowelling of the surface) and chemical (treatment of the surface with acid). With such treatment, the surface of material remains hydrophobic, saving the initial properties that a material possessed before the hydrophobic coating was applied [21].

The apparent contact angle (CA) is the principal parameter which characterizes the wetting properties of the surface. When the CA is less than 90°, it shows the hydrophilicity, which is the tendency of a surface to absorb water, while the CA greater than 90° indicates the hydrophobicity (water repelling). The super-hydrophobicity

corresponds to an apparent CA more than 150°. The CA between 120 and 150° indicates over-hydrophobic state [15]. Figure 1.5 illustrates the schematics of water droplets on the hydrophilic and hydrophobic surfaces.

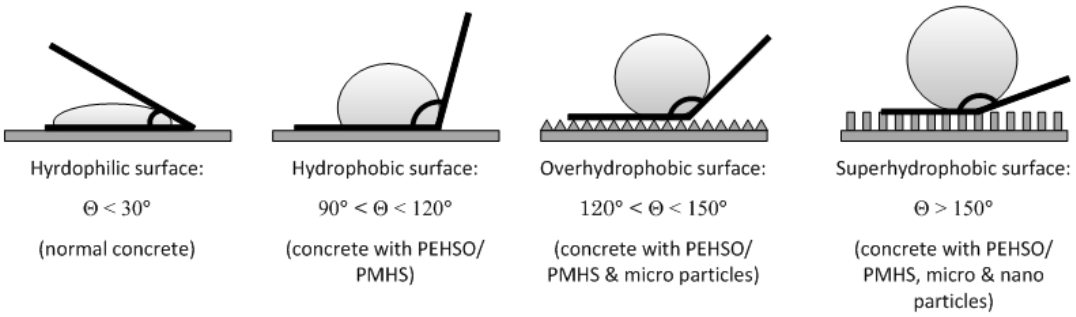

Figure 1.5. The hydrophilic (0° ≤ θ ≤ 90°), hydrophobic (90° ≤ θ), over-hydrophobic (120° ≤ θ < 150°), and superhydrophobic (150° ≤ θ ≤180°) surfaces, where θ is the CA [15]

A superhydrophobic coating is a nanoscopic surface layer that reflects the water. Different materials can be used to produce the superhydrophobic coatings, Figs. 1.6 and 1.7. The following compounds are known possible types of the coating [11, 17, 22, 28]:

- Silica nano-coating;
- Manganese oxide polystyrene nano-composite;
- Carbon nanotube structures;
- Zinc oxide polystyrene nano-composite;
- Precipitated calcium carbonate.

Silica nano-coatings are probably the most effective to use because can be easily applied via aerosol spray or by dipping the object into the gel [3, 30, 38]. Hydrophobic silica is a form of silicon dioxide that has hydrophobic groups chemically bonded to the surface. Hydrophobic silica demonstrates water-repellent properties because of its nanostructure and chemical properties. When the coating is applied on a surface of a material, the nanoparticles adhere to the material and prevent water from permeating the

texture. So water comes into contact only with the tips of the coating [3]. As a result, water is repelled from the coating due to the lack of attraction.

The general property of the main types of organo-silicate compounds is the presence of active functional groups that can chemically bind to the surface. Organocalcium siloxanes and silicon polymers with Si-O-Si group, chemically fixed on the surface of materials according to Figure 1.6 (a), hydrophobize the pores forming a hydrophobic film. Figure 1.7 illustrates the schematics of how randomly distributed polyvinyl alcohol (PVA) fibers embedded in the porous material can be used to achieve the superhydrophobicity [15].

The example of widely used organo-silicate compounds is represented by the alkyl-silicates, the structural formula of which is illustrated in Figure 1.6 (b). Being applied on the surface of the material, the sodium oxide reacts with the compounds on the surface and binds the silicate to the surface, and free radicals repel the water [3].

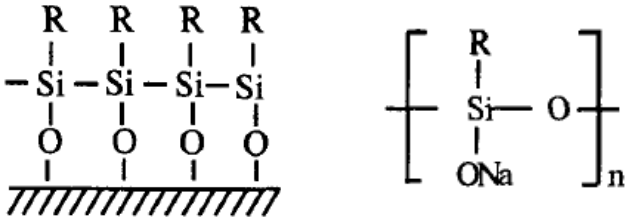

(a) **b)**

Figure 1.6. The chemical bonding of organocalcium siloxanes and silicon polymers with Si-0-Si group to the surface of the material (a) and the structural formula of the alkyl silicate organic compound (b) [3]

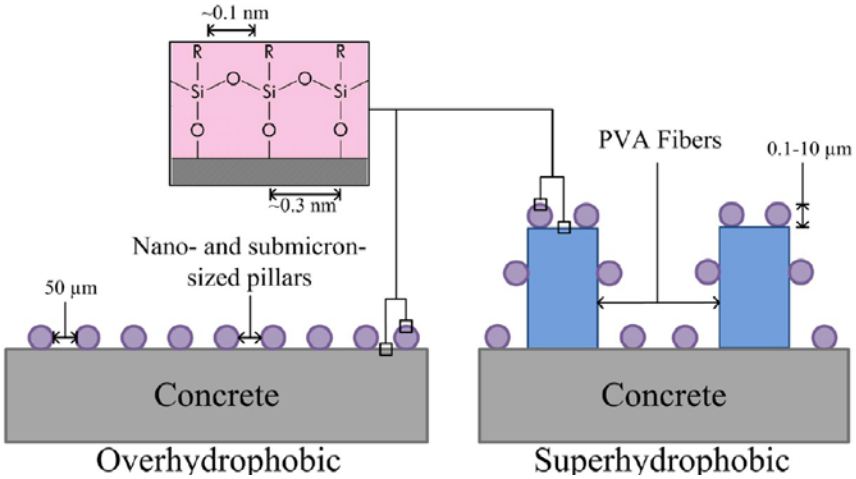

Figure 1.7. Schematics of the over-hydrophobic and superhydrophobic concrete [15]

2. Materials and Methods

2.1. Materials used in the experiment

Titanium dioxide

During the experiment, P25 titanium dioxide from Evonik was used as a photocatalyst, because it has the highest efficiency in the degradation of organic compounds and is often used as a reference material. The P25 titanium dioxide is a fluffy white hydrophilic powder with a specific surface area of 50 ± 15 m^2/g, the tapped density is 130 g/l, sieve residue (Mocker, 45 μm) ≤ 0.05 %, pH of 3.5 - 4.5. The boiling temperature of TiO_2 is 2,972 °C, and the melting temperature is 1,843 °C. The chemical composition of P25 includes TiO_2 ≥ 99.5 %, SiO_2 ≤ 0.2 %, Al_2O_3 ≤ 0.3 %, Fe_2O_3 ≤ 0.01 %, HCl ≤ 0.3 %. Figure 2.1 illustrates the X-ray diffractogram of the titanium dioxide based P25 product used in this research.

The maximum allowable concentration of titanium dioxide in the air of the working space is 10 mg/m³. Titanium dioxide is fire-and explosion-proof and not subjected to thermal destruction.

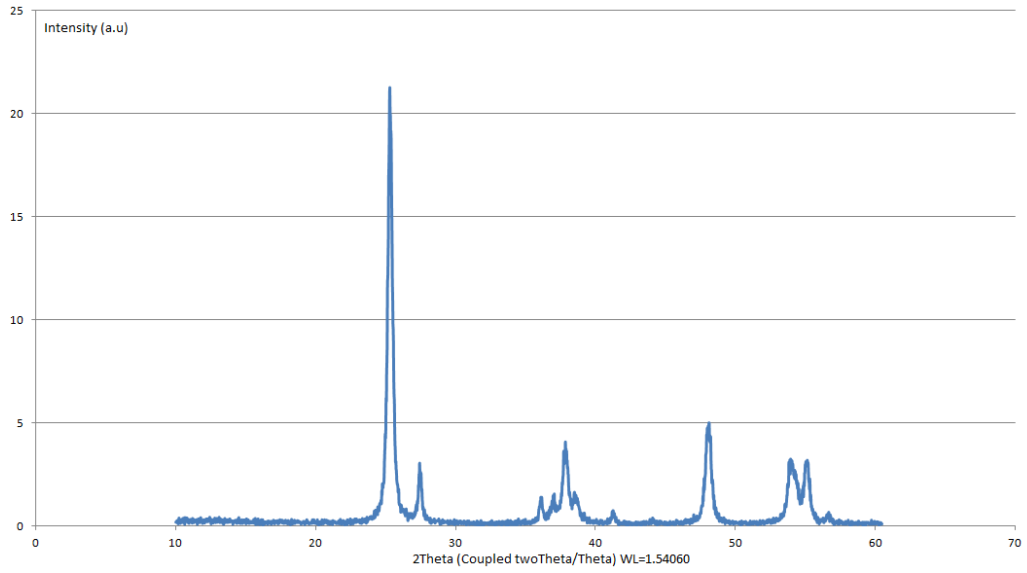

Figure 2.1. X-ray diffractogram of P25 titanium dioxide

Phosphoric acid

The chemical reagent grade phosphoric acid, containing 85 % of H_3PO_4 (and 15 % of water) in solution, was used as a component of the binder. The reagent is a clear, colorless and odorless viscous liquid with a density of 1.685 g/ml. The orthophosphoric acid is soluble in water (446 g/100 mL at 14.95 °C), has a boiling point equal to 133 °C, and a melting point equal to 42 °C.

Phosphoric acid reacts with aluminum, alloys of aluminum, and carbon steel. Therefore, stainless steel containers were used for the sample testing.

Ceramic tiles

The developed coatings were applied on the surface of unglazed ceramic tiles and tested for friction, photocatalytic properties, and hydrophobic properties. Thermal expansion of the tiles is low (1-15 ppm/°C), and melting point is high (600-4,000 °C). Ceramic tiles are also hard, rigid and brittle. The microstructure includes the grains, secondary phases, grain boundaries, micro-cracks, pores and structural defects.

One side of the tile has a smooth surface, therefore the coating was applied evenly on this surface by dipping the tiles into the solution. Ceramic tiles have a good water absorption, thermal stability, wear resistance, good chemical resistance to weak acids, such as phosphoric acid. Before the application of the coating, ceramic tiles were saturated with water to reduce the absorption of water from the coating solution.

Water-based siloxane emulsion

The water-based siloxane emulsion was used as a hydrophobic component of the coating. The emulsion consists of several components. Water-soluble polyvinyl alcohol (PVA) was used for emulsion stabilization agent, because of its perfect compatibility with concrete materials and non-ionic character. A highly hydrolyzed (98 %) PVA with a

molecular weight of 16,000 was used to reduce the foam formation. Polymethyl-hydrogen siloxane oil, PMHS (XIAMETER MHX-1107) with a viscosity of 30 cSt and a specific gravity of 0.997 (at 25 °C) was used as the hydrophobic agent. This product contains 85 − 100 % of methyl-hydrogen siloxane as an active agent. Deionized water was used as the dispersion medium.

The concentration of siloxane and surfactant was kept constant at 25 and 4.4 %, respectively, by the weight of the emulsion [15]. A high-speed mixer (HSM, model L5M-A from Silverson) was used to prepare the emulsions using the procedure described by Flores-Vivian et al [15]. For the solution preparation, PVA was gradually added to deionized water and stirred, using a magnetic stirrer with a hot plate, for 10 min at 23 ± 3 °C to avoid clumping. Then, the temperature was increased to 95 ± 2.5 °C, and kept constant for 40 min while stirring to achieve complete dissolution. The solution was cooled in a water bath until a temperature of 23 ± 3 °C. To stabilize the emulsions, high speed and high shear mixer at 10,000 rpm was used to produce the small droplet size [15]. The emulsions were characterized by an optical microscope (Olympus BH-2) at 1,000X magnification.

Deadly burned magnesium oxide

Deadly burned magnesium oxide was used in the experiment to explore the possibility to create a durable coating without heat treatment. Magnesium oxide is a white solid mineral and deadly burned magnesium oxide is manufactured at a relatively high temperature of 1500ºC – 2000ºC. This material has a very little reactivity.

2.2. Experimental methods

Confocal Laser Scanning Microscopy (CLSM)

The tiles covered with the coating were observed under the confocal laser scanning microscopy (CLSM) with 20X magnification to inspect the formation of cracks and their dependence on the temperature treatment.

The CLSM is an optical imaging technique used to increase the optical resolution and contrast of a micrograph by using a spatial pinhole to block the out-of-focus signal when the image is formed. Capturing multiple 2D images at different depths on a sample enables the reconstruction of 3D structures [24]. The thin optical sectioning makes this technique applicable for 3D imaging and surface profiling of samples.

The CLSM achieves a highly limited and controlled depth of focus. The confocal microscope only focuses a smaller beam of light at one narrow depth level at a time, and only the in-focus is recorded, while, under the conventional microscope, light travels through the sample as far as it can penetrate.

Under the CLSM, the beam is scanned across the sample in the horizontal plane by the oscillating mirrors. This scanning method has a low reaction latency. Slower scans provide a better signal-to-noise ratio, resulting in better contrast and higher resolution [24].

Scanning Electron Microscope (SEM)

A scanning electron microscope (SEM) was used to investigate, how the coating binds to the surface of ceramic tiles and whether free particles of titanium dioxide remain on the surface of the coating.

The SEM is a type of electron microscope that produces images by scanning the surface of a sample with a focused beam of electrons. SEM micrographs have a large depth of field due to the very narrow electron beam. Therefore, scanning electron

microscopes yield a three-dimensional appearance important for understanding the surface structure of a sample.

Thermal Treatment

The thermal treatment of the samples was carried out using a muffle furnace that allows to set the required temperature and to change the temperature at any time when it is necessary. All samples were placed to the muffle furnace right after the coating was applied and the tiles were treated at 250 ˚C during processing time up to three hours.

X-ray Diffraction

The chemical compositions of the coatings were determined using the X-ray diffraction method. X-ray scattering technique is a technique used for determining the information about the chemical composition, crystal structure, and physical properties of materials. This technique is based on reporting the scattered intensity of an X-ray beam hitting a sample. The beam of incident X-rays, achieving the crystalline atoms, diffracts into many specific directions. By measuring the angles, intensities, polarization, wavelength or energy of these diffracted beams, the X-ray diffractor produces the two-dimensional graphs of the intensities of electrons within the crystal.

The photocatalytic degradation of NO_x

To determine the factors, influencing the photodegradation of the organic compounds, the photocatalytic reaction was imitated in the laboratory. During the experiment, the sample was placed in a chamber covered with a thin film that made the chamber seal and allowed the ultraviolet irradiation to pass directly through to the chamber. The source of ultraviolet irradiation was located at the distance of 36 cm from the surface of the sample. The air humidifier was connected to the chamber. The

ventilator was placed into the chamber for better mixing of deposited gas and air. Figure 2.2 illustrates the schematics of the equipment.

The NO gas mixed with air in fixed proportions went to the chamber through the pipeline attached to the chamber and then went to the NO_x analyzer. At the beginning of the experiment, the source of the ultraviolet irradiation was turned off. The NO analyzer measured the steady state flow concentration of NO and NO_x, and after that, the source of UV irradiation and the humidifier were turned on. The photocatalytic reaction processed in the chamber, when the tested samples were under the UW irradiation. Here, the NO analyzer can detect the reduction of NO and NO_x concentrations. When the final concentrations of NO and NO_x were stabilized, the source of UV irradiation and the humidifier were turned off. At that moment, the concentration of gases increases rapidly due to a constant supply of NO. The stabilized data, reaching the initial levels, were recorded by the NO analyzer.

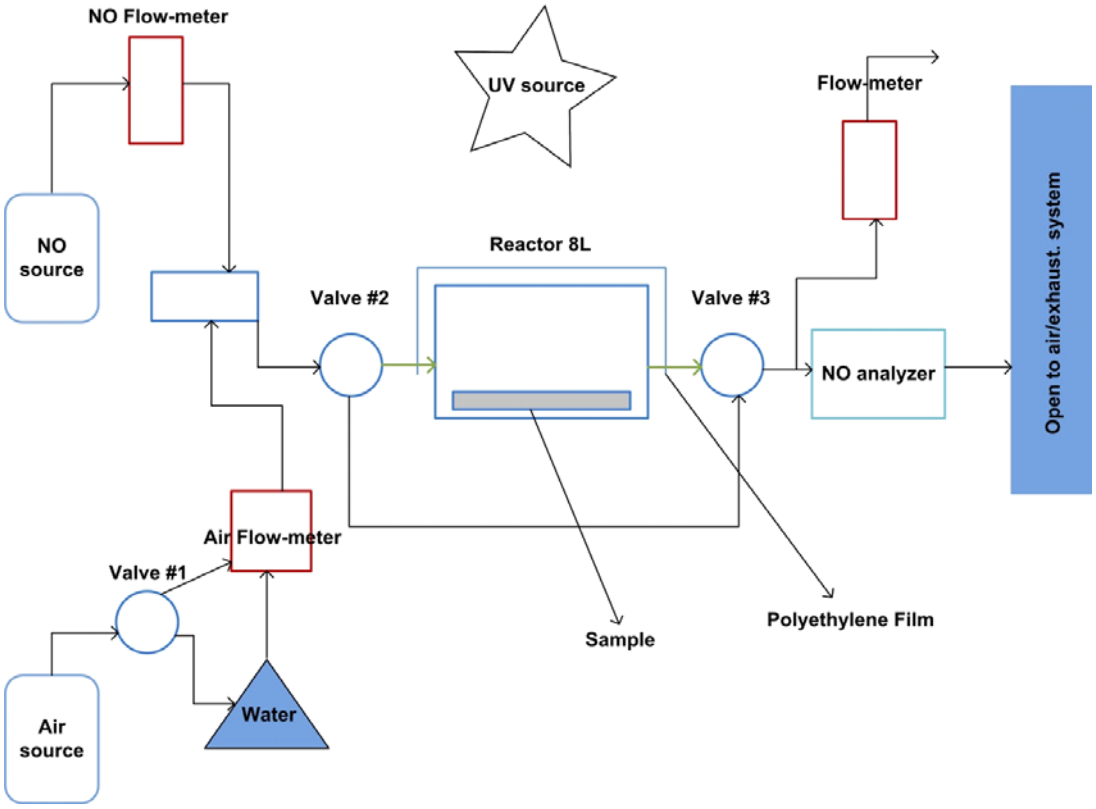

Figure 2.2. Schematics of the photocatalytic degradation experiment

Friction Tribometery

The adhesion and structural integrity of the coating to the surface of the tiles were tested on the friction tribometer. A tribometer is the instrument that measures the tribological quantities, such as friction force, the coefficient of friction, and wear volume, between two surfaces in contact.

A tribometer principles were described by the manufacture as a hanging mass and a mass resting on a horizontal surface, connected to each other via a string and pulley. The coefficient of friction μ is determined by increasing the hanging mass until the moment that the resting mass begins to slide [39].

The general equation for friction force:

$$F = \mu N \quad [1]$$

where

F - the loading force, equal to the weight of the hanging mass (m_H), (N)

μ - coefficient of friction,

N - the normal force, equal to the weight (mass x gravity) of the sitting mass (m_T).

thus, $\mu = m_H/m_T$.

The applied load was 25 N. The nitrile rubber was used for testing of friction coefficient as a material, which contacts with the surface of the coating.

Measuring the Contact Angle

The wetting properties of the coating were investigated by measuring the water CA using the Ramé-Hart Goniometer model 250. At least three 5 μL water droplets were placed at different points on each sample. The siloxane based emulsion was used to achieve hydrophobicity. The images of water droplets as well as the values of water CAs on different hydrophobic coatings are reported in Figure 4.5.

3. Experimental Program and Results

3.1. Objectives

The main objective of the research program was to create a new durable photocatalytic and also hydrophobic coating. This coating can be applied to concrete pavements and other structures to reduce the air pollution and also to protect the structures from the destruction due to the expansion of water in pores after multiple freeze-thaw cycles. To achieve this goal, two-stage method, comprising of the formation of photocatalytic nanoparticle layer, chemically bonded to the substrate, and siloxane coating on the top of the photocatalytic surface, forming the hydrophobic structure, is proposed.

The experimental program included the optimization of chemical composition, the concentrations of components and methods of application of the coating. The formation of titanium phosphates was proposed as a method of nanoparticle attachment. However, it was necessary to prove that such coatings can demonstrate the same photocatalytic properties as the reference titanium dioxide. Also, it was necessary to determine how the hydrophobic water-based siloxane emulsion can affect the photocatalytic properties of developed coatings. Since the hydrophobic component may reduce the catalytic effect of the coating, the influence of siloxane emulsion on the self-cleaning properties was investigated. The resulting two-stage coating should have good adhesion to the surface of brick and concrete and have good durability, possessing abrasion-resistant properties.

3.2. Preliminary experimental matrix

Several experimental matrixes were designed to optimize the concentrations of components of the coating, methods of application and to identify the factors, which have the most significant influence on the performance of developed coatings. The main criteria to create the coating were the water/H_3PO_4 ratio, TiO_2/H_3PO_4 ratio, the temperature of the heating and the type of heating. Table 3.1 characterizes the solutions that were created and tested in the first stage of the experiment. The basic equation to obtain the optimal proportions of components of the coating is:

$$4H_3PO_4 + 3TiO_2 = 6H_2O + Ti_3(PO_4)_4 \quad [2]$$

Based on this equation, the optimal proportions, assuming that the phosphoric acid and titanium dioxide entirely react, are equal to 64 % of the phosphoric acid and 36 % of the titanium dioxide, by weight (see Table 1.2). In the experiments described in Table 3.1, the water/H_3PO_4 ratio was two or three, and the TiO_2/H_3PO_4 ratio was one or three of the required amount (36/64) according to the Equation 2.

Table 3.1. The matrix of a preliminary experiment

№ of Sample	TiO_2/H_3PO_4, by weight	Water/ H_3PO_4, by weight	The temperature of Heating, °C
P1	1	2	25
P2	1	2	250
P3	1	3	25
P4	1	3	250
P5	3	2	25
P6	3	2	250
P7	3	3	25
P8	3	3	250

When the TiO_2/H_3PO_4 ratio is three times of the stoichiometric ratio according to the Equation 2, a part of the titanium oxide does not react with the acid, and this can ensure

the attainment of photocatalytic properties. The optimal water amount in the solution should be obtained to provide the appropriate fluidity, uniformity of coating and required density of particle coverage. Dense solutions may result in thick coatings and even cracks on the surface of the coating. Half of the resulting compositions was subjected to thermal treatment in the oven at 250 °C, which is the optimal temperature for the reaction according to the Equation 2 [14]. The rest of the compositions was cured at room temperature (25 °C).

3.3. Preliminary results and evaluations

The influence of thermal treatment on properties of the coating

The chemical transformations in the investigated system were evaluated using the XRD patterns. Figures 3.3 and 3.4 illustrate the XRD patterns of samples P2 and P6, respectively, treated at 250 ˚C and compared with reference coatings (samples P1 and P5). It can be confirmed that phosphoric acid does not react with the titanium dioxide at a room temperature, which was evidenced by other researchers [14]. Thus, for the future research, all samples were treated at a temperature of 250 ˚C.

The influence of dilution rate on properties of the coating

The excess amount of water in the solution can not influence the reaction of the titanium dioxide with the phosphoric acid critically but may influence the physical and mechanical properties of the coating. Fluid solution can result in a uniform coating with fewer shrinkage cracks, which was observed under the microscope, but higher water content can result in the increased porosity and reduced strength (Table 1.2).

For the preliminary experimental program, two different water/H_3PO_4 ratios of 2 and 3 were implemented. Figure 3.2 illustrates the cracks on the surface of the coating observed under the confocal microscope when water/H_3PO_4 ratio was equal to 3. This

pattern was compared with the results for the uncoated surface of the reference ceramic tile, illustrated in Figure 3.1. The resulting compositions had a high density and reduced fluidity. Thus, the dilution rate was increased by 10 times to make fluid solutions, so the water/H_3PO_4 ratio in the experiment was set to be 20 or 30 (by weight).

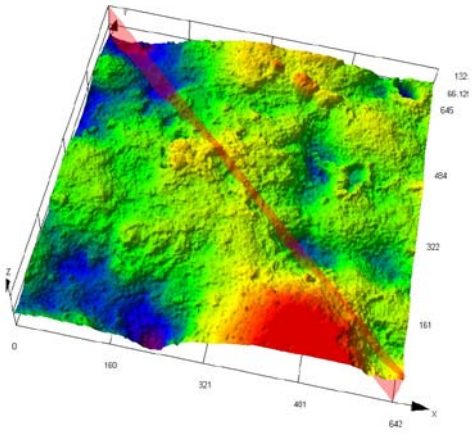

Figure 3.1. Uncoated surface of the reference ceramic tile observed under the confocal microscope with 20X magnification

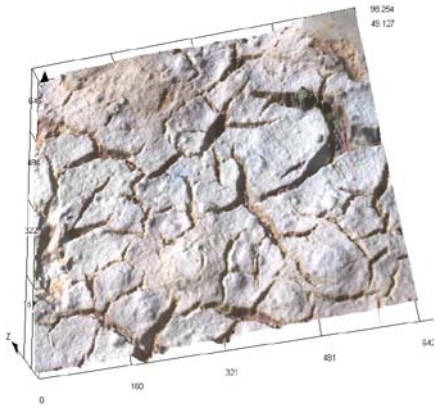

Figure 3.2. Cracks on the surface of the coating observed under the confocal microscope with 20X magnification

The influence of TiO_2/H_3PO_4 ratio on properties of the coating

As discussed above, if the TiO_2 concentration exceeds the required amount for the complete reaction with the phosphoric acid, a part of TiO_2 will remain unreacted, providing the catalyst on the surface of the coating. In this case, the TiO_2 particles can remain available for photocatalysis and create free radicals, decomposing the harmful

gases in the air. Therefore, in the experiment, two different amounts of TiO_2 were used: the stoichiometric ratio (36 % of TiO_2 and 64 % of H_3PO_4 by weight) and three times over the stoichiometric ratio. Figures 3.3 and 3.4 report on the XRD for samples P2 and P6, respectively. Figure 2.1 reports on the XRD pattern of P25 titanium dioxide used as a reference for the research.

The XRD can identify the picks characterizing TiO_2 rutile and TiO_2 anatase. The sample P6 demonstrates higher intensity for the titanium dioxide than sample P2, which means that sample P6 has the higher concentration of free TiO_2 particles than sample P2. Here, it is proved that a portion of the titanium dioxide did not react with H_3PO_4 saving the photocatalytic properties of the coating.

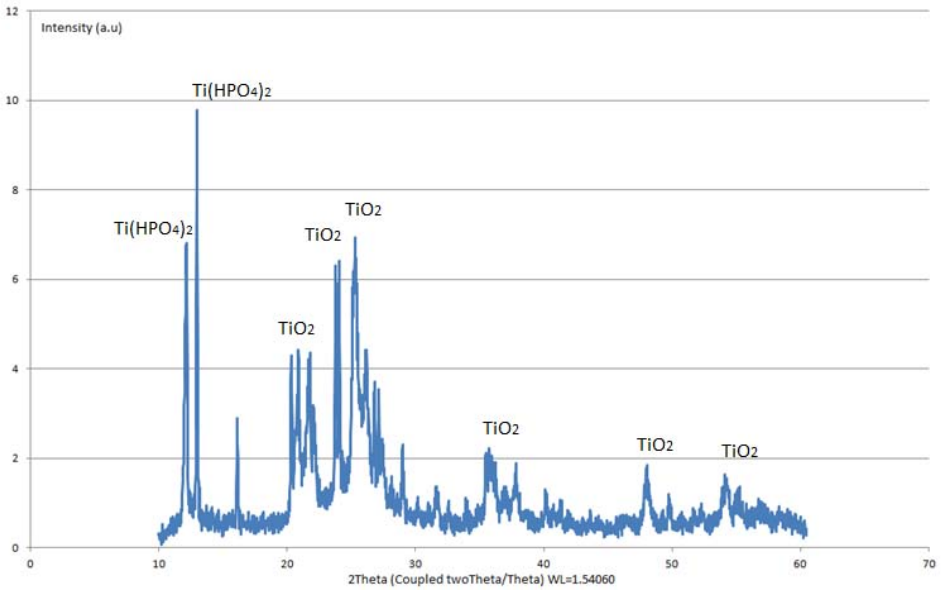

Figure 3.3. X-ray diffractogram of sample P2

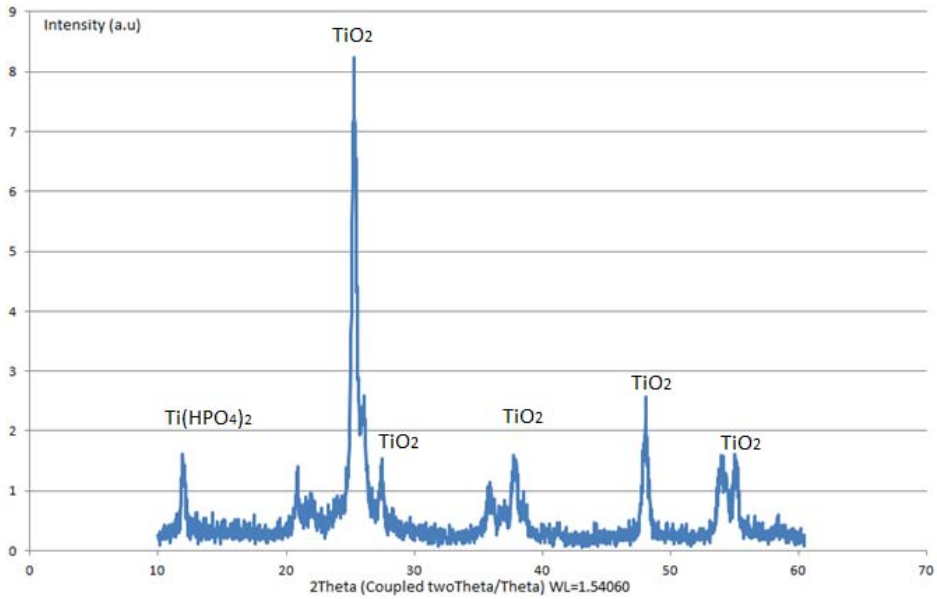

Figure 3.4. X-ray diffractogram of sample P6

The formation of phosphates

The XRD patterns identify that sample P2 has the high concentrations of titanium phosphates, such as the titanium hydrogen phosphate and titanium hydrogen phosphate hydrate. The sample P6 also has titanium phosphates in lower concentrations, which proves that phosphate reaction took place at 250 °C, and a part of the titanium dioxide particles reacted with the phosphoric acid. A hard solid structure of resulting material proves that the titanium phosphates were formed, which can be strongly adhered to the substrate.

3.4. Influence of magnesium oxide on the titanium phosphate formation

The experiment was conducted to investigate the influence of MgO on the properties of the coating. Magnesium phosphates do not require any thermal treatment for hardening, while titanium phosphates harden at high temperatures. Thus, the objective of the experiment was to explore the possibility to create a durable coating without heat treatment using magnesium oxide component. Table 3.2 describes the

experimental matrix, which has two criteria varying among the samples: TiO_2/H_3PO_4 ratio and MgO/TiO_2 ratio.

Table 3.2. Experiment matrix for the samples with magnesium oxide

№ of experiment	TiO_2/H_3PO_4 by weight (of 34/66)	MgO/TiO_2 by weight
M1	1	0.1
M2	1	0.2
M3	3	0.1
M4	3	0.2

In the experiment, the optimal TiO_2/H_3PO_4 ratio (34 % of TiO_2 and 66 % of H_3PO_4) and triple the optimal TiO_2/H_3PO_4 ratio were applied. The MgO/TiO_2 ratios equal to 0.1 and 0.2 by weight were used. The amount of water in each case was calculated as three times the amount of phosphoric acid by weight. The titanium dioxide, and magnesium oxide were mixed with diluted phosphoric acid (acid was added to water). The components were mixed, and the resulting mixtures were treated at a room temperature of 25 ˚C. The resulting compositions were investigated using XRD to determine the composition of products of the reaction. The XRD pattern of the reference magnesium oxide is given in Figure 3.5. Figure 3.6, Figure 3.7, Figure 3.8 illustrate the XRD patterns of samples M2, M3, and M4, respectively. Sample M1 did not harden at room temperature and was not tested on X-ray diffractor.

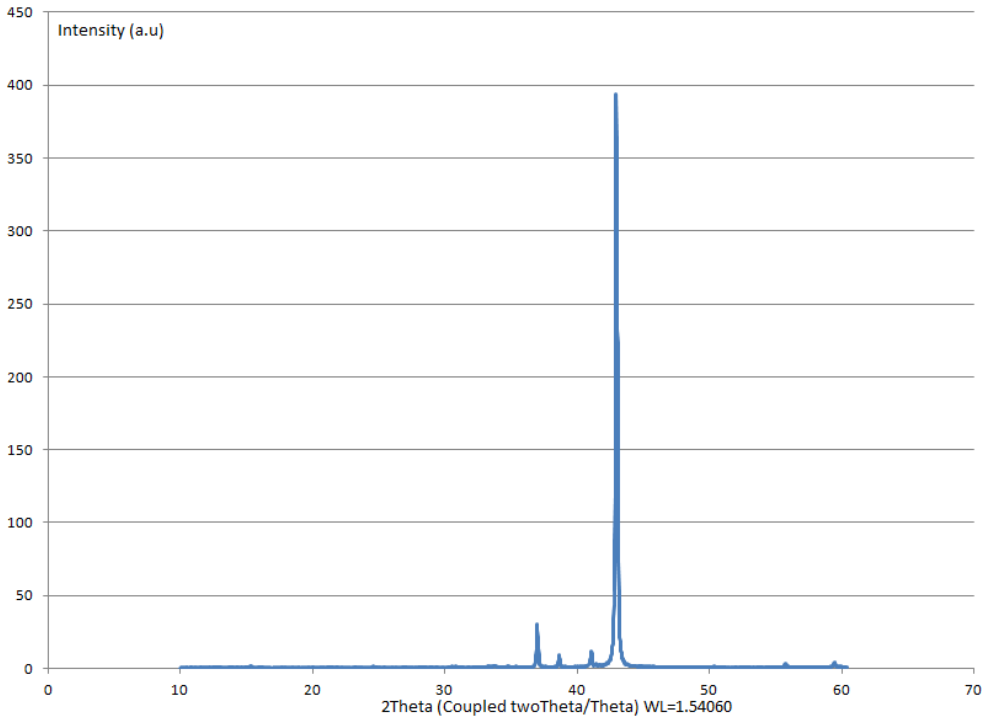

Figure 3.5. X-ray diffractogram of the reference magnesium oxide component

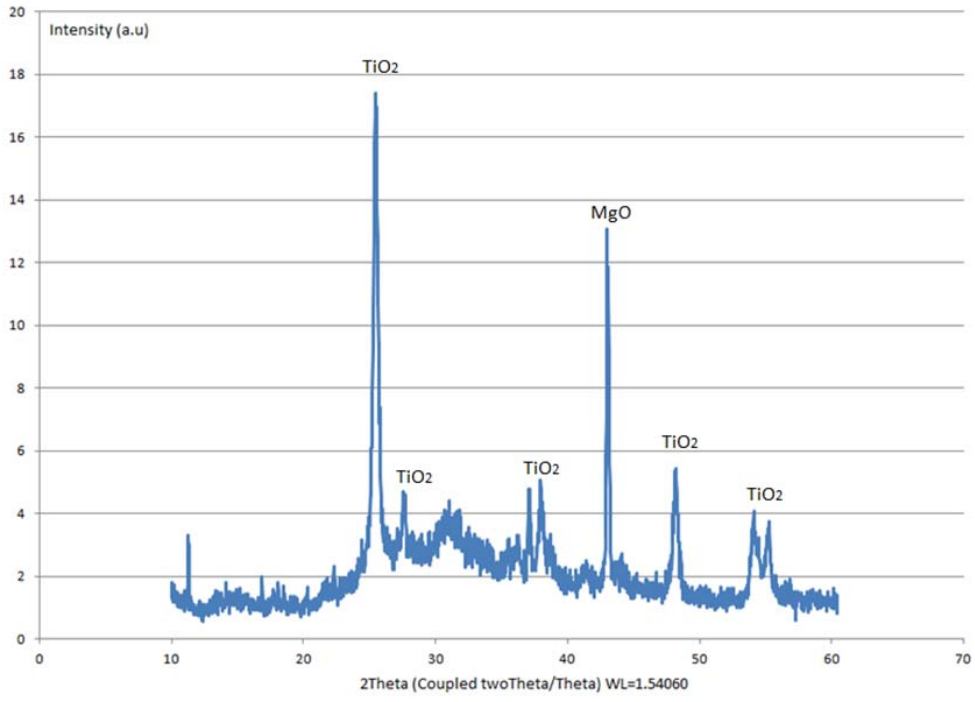

Figure 3.6. X-ray diffractogram of sample M2

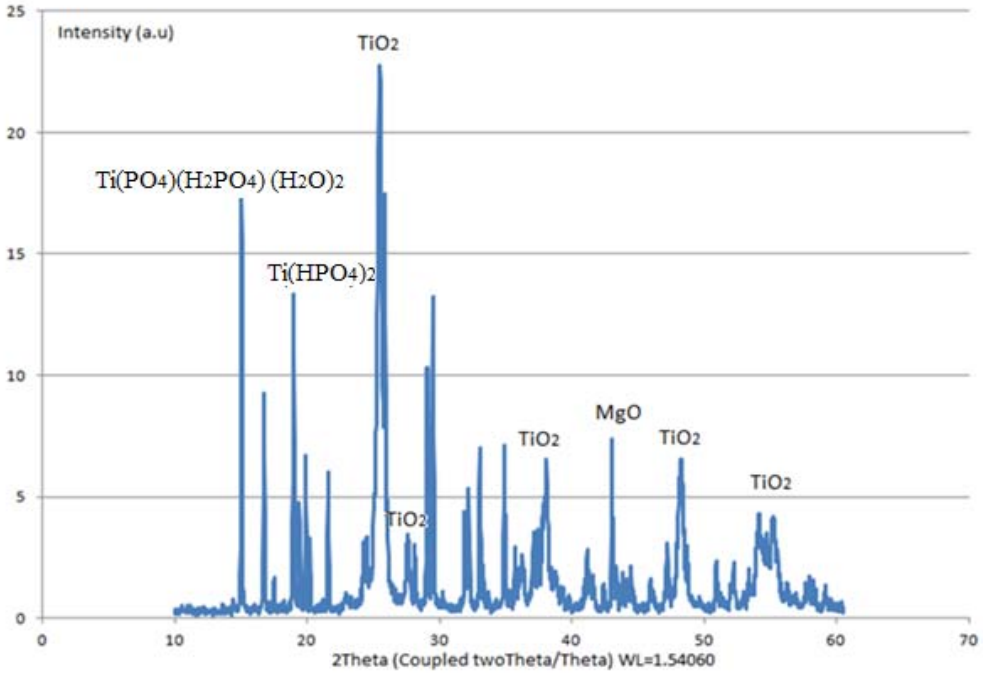

Figure 3.7. X-ray diffractogram of sample M3

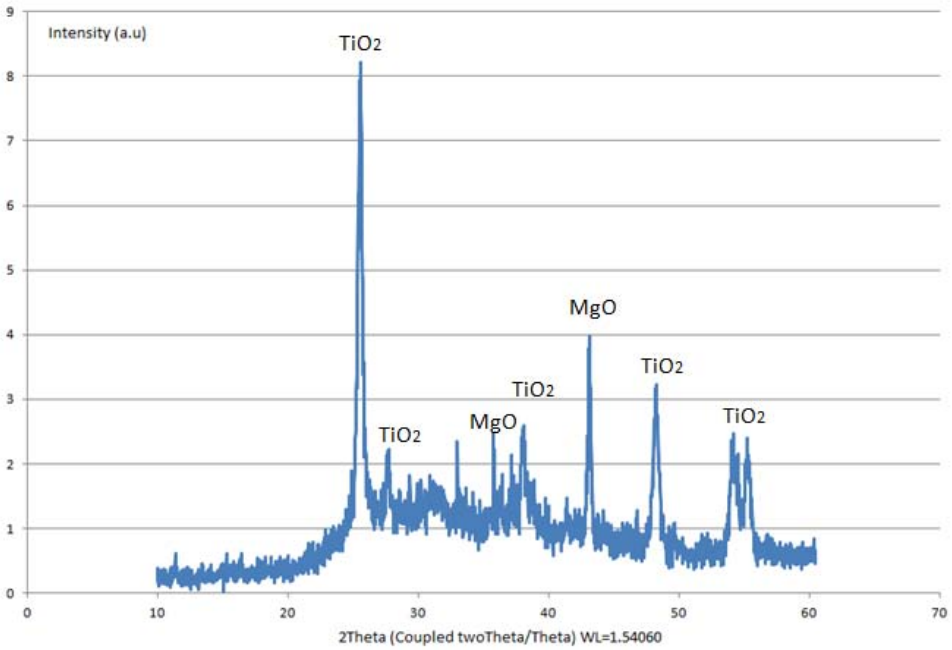

Figure 3.8. X-ray diffractogram of sample M4

X-ray diffractograms of samples M2, M3 and M4 demonstrate many clearly expressed picks, not related to the reference magnesium oxide, which means that different types of phosphates and hydrates were formed in the compositions. However, all resulting samples had a crumbled structure, and expected strength of the material was

not achieved. In these cases, magnesium oxide played the role of the passivator for the formation of the initial solid component.

Although phosphates were formed at room temperature for samples M2, M3 and M4, the presence of MgO in the coating was found to reduce the mechanical properties significantly. Compositions and proportions used in the research did not result in strong coatings, and so were not recommended for the consequent use. For this reason, the use of MgO for the formation of titanium phosphates was not justified, and further experiments were conducted using the titanium dioxide and phosphoric acid.

3.5. The design of refined experimental matrix

The refined experimental matrix was designed taking into the account the following factors, which may have an influence on photocatalytic properties, the formation of shrinkage cracks on the surface and the abrasion resistance of the coating such as time of heating and cooling regimes, water/H_3PO_4 ratio, TiO_2/H_3PO_4 ratio and the flow/concentration of NO_x to be decomposed. Table 3.3 summarizes the refined experimental matrix. The second hydrophobic coating was applied to the primary coating after the optimal compound layer was obtained.

Table 3.3. Refined experiment matrix

№ of Sample	Duration of Heating-Cooling, hours	Water/P.Acid Ratio	TiO_2/P.Acid Ratio	The concentration of NO, ppm	NO Flow, l/min (at air 1.4 l/min)
R1	1	20	4	2.7	0.06
R2	1	20	4	1.5	0.03
R3	1	20	2	2.7	0.06
R4	1	20	2	1.5	0.03
R5	1	30	4	2.7	0.06
R6	1	30	4	1.5	0.03
R7	1	30	2	2.7	0.06
R8	1	30	2	1.5	0.03
R9	3	20	4	2.7	0.06
R10	3	20	4	1.5	0.03
R11	3	20	2	2.7	0.06
R12	3	20	2	1.5	0.03
R13	3	30	4	2.7	0.06
R14	3	30	4	1.5	0.03
R15	3	30	2	2.7	0.06
R16	3	30	2	1.5	0.03

The first factor, duration of heating and cooling, may influence the formation of cracks on the surface. The structure of cracks of resulting coatings was observed under the confocal microscope. Water/H_3PO_4 ratio from 20 to 30 by weigh allows the attainment of a fluid solution used for the coatings. Also, the use of different water/H_3PO_4 ratios may influence the photocatalytic properties in different ways. For this subset, the TiO_2/H_3PO_4 ratios were taken at 2 and 4 (over the 34/66). Also, two different initial concentrations of NO_x equal to 2.7 ppm and 1.5 ppm were used, which may influence the conversion of NO_x. The last column of Table 3.3 describes the flow of constituents to obtain the required concentrations of NO_x. All coatings were applied on

the ceramic tiles, and these tiles were tested for crack formation, photocatalytic properties and coefficient of friction.

3.6. The influence of heating and cooling on the formation of cracks

The samples R1-R8 were heated in a furnace for 1 hour at a constant temperature of 250˚C. Such rapid heating may lead to the additional crack formation on the surface upon coating. These cracks may lead to exfoliating of the coating from the surface of the material. Figure 3.9, Figure 3.10 and Figure 3.11 represent the CLSM images of samples R2, R5, and R7, respectively.

Since cracks were observed on the surface of sample R2, a new protocol for thermal treatment was developed to investigate the possibility to reduce the crack formation by changing the heating and cooling regime. Figure 3.12 represents the regime of heating and cooling for the samples R8-R16. During the first hour, the temperature increases evenly from 25 ˚C to 250 ˚C. During the second hour, the temperature is constant and equal to 250 ˚C. After this, the temperature decreases gradually from 250˚C to 25˚C during 3rd hour.

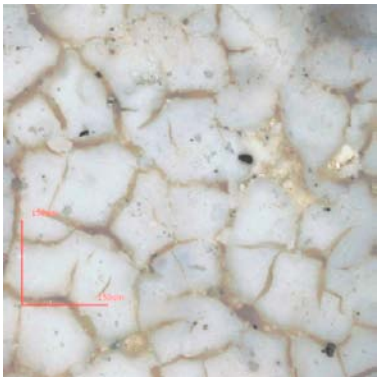

Figure 3.9. Cracks on the surface of the coating observed under the confocal microscope with 20X magnification for sample R2

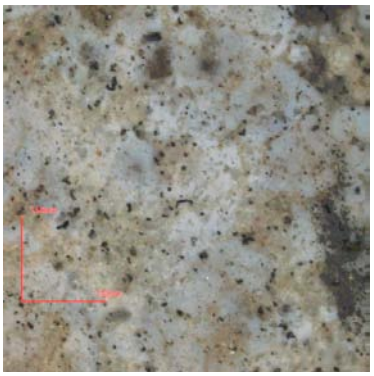

Figure 3.10. The surface of the coating observed under the confocal microscope with 20X magnification for sample R5

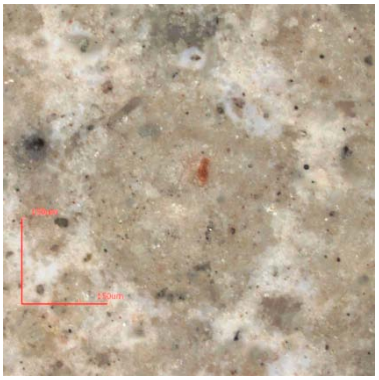

Figure 3.11. The surface of the coating observed under the confocal microscope with 20X magnification for sample R7

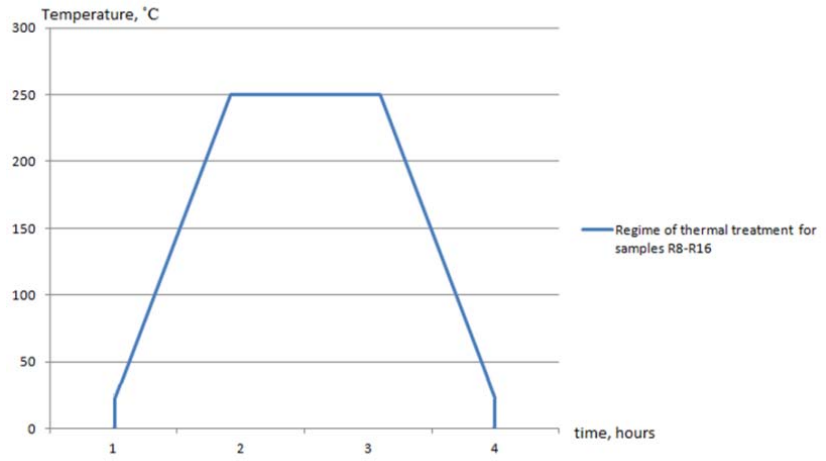

Figure 3.12. The regime of thermal treatment for samples R8-R16

The coatings R9-R16 subjected to thermal treatment during three hours were investigated under the confocal microscope to detect the formation of cracks. Figure 3.13 represents the CLSM images of cracks on the surface of the sample R9.

The images in Figure 3.13 demonstrate that slow heating and cooling did not have a significant influence on the crack formation. It can be seen that the coating was not applied on the surface of the tile evenly. There are some places with thinner and thicker layers. The cracks are observed only on thick layers. Thus, to prevent the formation of cracks, evenly distributed thin layer should be applied on the surface of the tile. To achieve this goal, the extremely diluted coating was tested. The heating and cooling regime for the optimal coating can be 250˚C used for one hour.

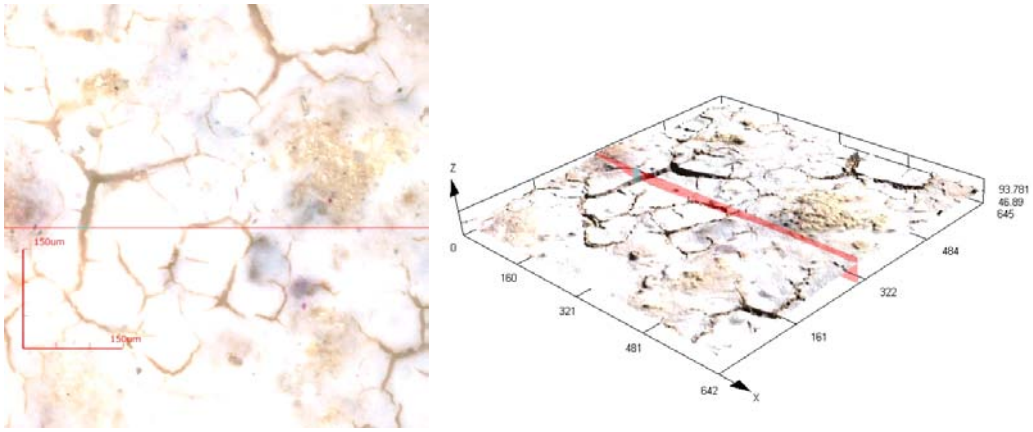

Figure 3.13. Cracks on the surface of the coating observed under the confocal microscope with 20X magnification for sample R9

3.7. Photocatalytic properties

The investigated coatings were applied on ceramic tiles and tested using NO/NO_x analyzer for photocatalytic properties. The surface area, covered with the coating and subjected to UV irradiation was 22,500 mm^2. During the experiment, the relative humidity in the chamber was 56.4 %. Figures 3.14-3.17 illustrate the NO_x decomposition for samples R1-R8 by recording the concentrations of NO and NO_x versus time. At the beginning of the experiment, the initial concentration is remaining at the preset level. With UV radiation, when the photocatalytic reaction takes place, the concentration of NO_x begins to reduce and reaches the steady level. Based on the experimental data, the reduction of NO_x concentration can be estimated.

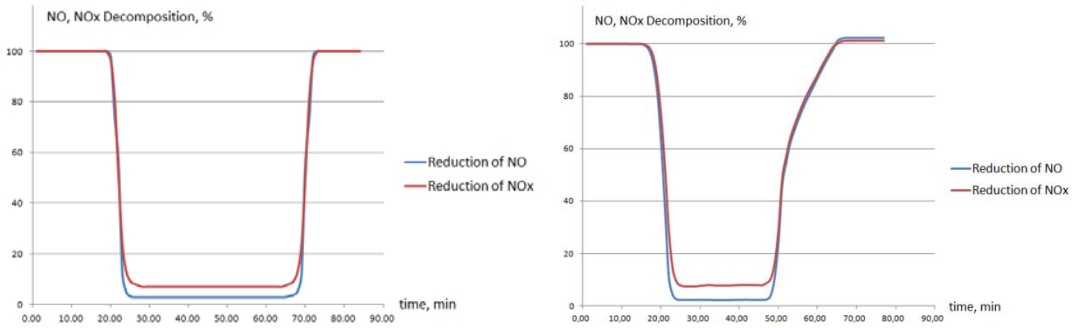

Figure 3.14. NO_x decomposition for sample R1/R2 at the NO_x concentration of 2.7 ppm (left) and 1.5 ppm (right)

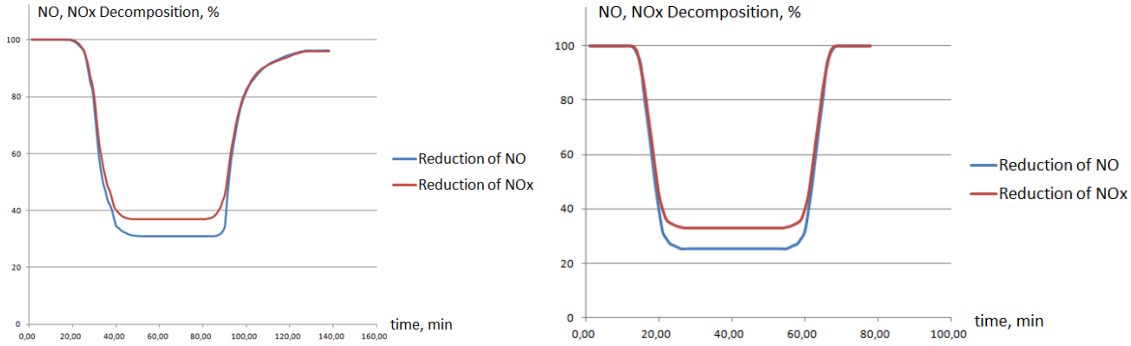

Figure 3.15. NO_x decomposition for sample R3/R4 at the NO_x concentration of 2.7 ppm (left) and 1.5 ppm (right)

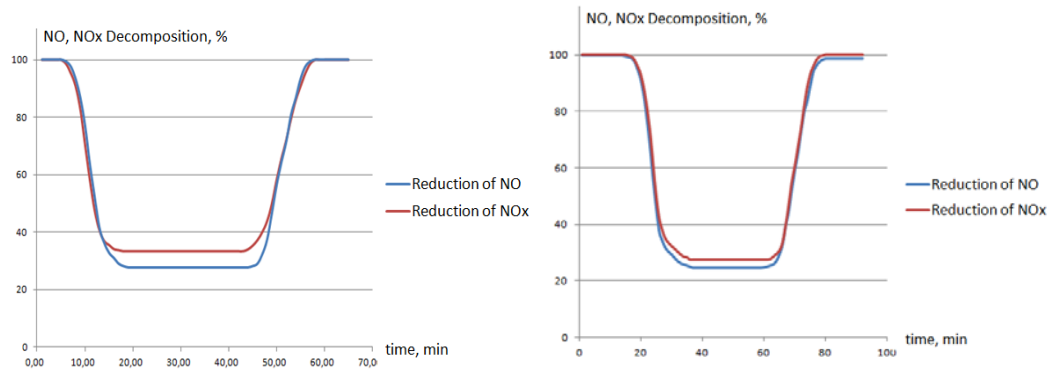

Figure 3.16. NO_x decomposition for sample R5/R6 at the NO_x concentration of 2.7 ppm (left) and 1.5 ppm (right)

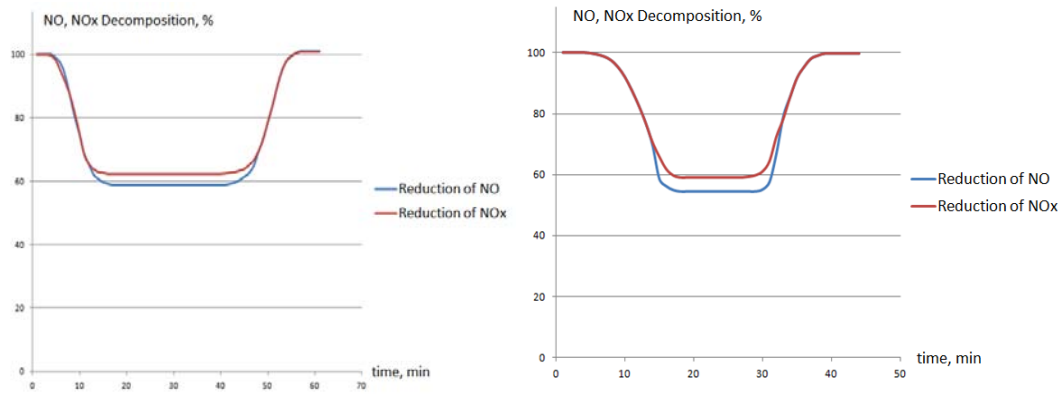

Figure 3.17. NO_x decomposition for sample R7/R8 at the NO_x concentration of 2.7 ppm (left) and 1.5 ppm (right)

All tested samples demonstrate very significant decomposition of NO_x. Table 3.4 reports on the reduction of NO and NO_x for the samples R1-R8.

Table 3.4. Decomposition of NO and NO_x for samples R1-R8

№ of Sample	Water/P.Acid Ratio by Weights	TiO_2/P.Acid Ratio	Initial Concentration of NO, ppb	Reduction of NO, %	Reduction of NOx, %
R1	20	4	2712	97	93
R2			1552	97	93
R3	20	2	2795	69	63
R4			1590	75	67
R5	30	4	2730	67	64
R6			1526	75	69
R7	30	2	2700	41	37
R8			1491	45	41

The influence of water/H_3PO_4 ratio on photocatalytic properties

Based on Table 3.4, the impact of various factors on the photocatalytic properties of the coating may be evaluated. The first factor, the water/H_3PO_4 ratio, has a significant effect on the degradation of NO and NO_x. Samples R5, R6, R7, R8, which were produced with a higher water/H_3PO_4 ratio, demonstrated lower degradation of NO and NO_x than the samples R1, R2, R3, and R4. The reason for this is that more diluted

solutions have less amount of titanium dioxide per unit volume (and area). Therefore, the concentration of titanium dioxide particles on the surface of covered tiles is reduced. Thus, less free radicals are generated during the photocatalytic reaction, and the NO_x decomposition decreases.

The results of the photocatalytic degradation for samples, which have the same characteristics and differ only in water/ H_3PO_4 ratios, demonstrate the average difference in degradation of NO gas equal to 27.5 %, and the average difference in degradation of NO_x is 26.3 %.

The influence of TiO_2/H_3PO_4 ratio on photocatalytic properties

The second factor, the TiO_2/H_3PO_4 ratio, also has a significant influence on the photocatalytic properties, based on Table 3.4. Samples R1 and R3 only differ in the TiO_2/H_3PO_4 ratio, and the sample R1 demonstrated a 28 % higher degradation of NO than sample R3. Sample R2 demonstrated a 22 % higher decomposition of NO and 26 % higher decomposition of NO_x than the sample R4. The sample R1 has twice as much titanium dioxide per unit weight as the sample R3. For this reason, the sample R1, after applying on the surface and hardening, may have more free titanium dioxide particles, which did not react with the phosphoric acid, than the sample R3. These free particles of TiO_2 increase photocatalytic properties of the coating.

Samples R5 and R7 demonstrate similar results. The sample R5 had a 38 % higher degradation of NO and 39 % higher degradation of NO_x than the sample R7. The results of the photocatalytic degradation for samples, which have the same characteristics and differ only in TiO_2/H_3PO_4 ratios, demonstrated the average difference in degradation of NO equal to 26.5 %, and the average difference in degradation of NO_x is 27.7 %.

The influence of initial NO_x concentration on photocatalytic properties

The initial concentration of NO_x also influences the photocatalytic degradation process. Based on the results in Table 3.4, if all other parameters are equal, samples demonstrate better photocatalytic properties at lower initial NO_x concentrations. For the samples with the same characteristics and the different initial concentrations of NO_x, the average difference in degradation of NO was equal to 4.5 %, and the average difference in degradation of NO_x was equal to 3.25 %.

Based on the results in Table 3.4, for this data, the water/H_3PO_4 ratio and TiO_2/H_3PO_4 ratio had the most significant impact on the photocatalytic degradation. However, all the samples demonstrated a high decomposition of NO and NOx. The desirable decomposition of NO_x is at least 30 %. Therefore, a composition with a lower TiO_2/H_3PO_4 ratio can be further developed and tested.

3.8. Tribological properties

One of the most significant factors, characterizing durable coating is the abrasion resistance. To be abrasion resistant, the coating must be solid, have a high hardness and good adhesion to the surface of the substrate. The test for the abrasion resistance was performed on the tribometer with an applied vertical load of 25 N. The nitrile rubber, connected to the hanging mass via a sting and applied to the surface of the coating, generated the friction force. The coefficient of friction, characterizing the abrasion resistance of the coating, was determined by dividing the friction force by the applied load. The uncoated ceramic tile was tested on the tribometer as a reference. The result of the tribological test for the uncoated ceramic tile is illustrated in Figure 3.18.

Samples R2, R5, R7, and R9, which differ in chemical composition and the thermal treatment regime were tested on the tribometer, and the results of the tests are illustrated by Figures 3.19-3.22.

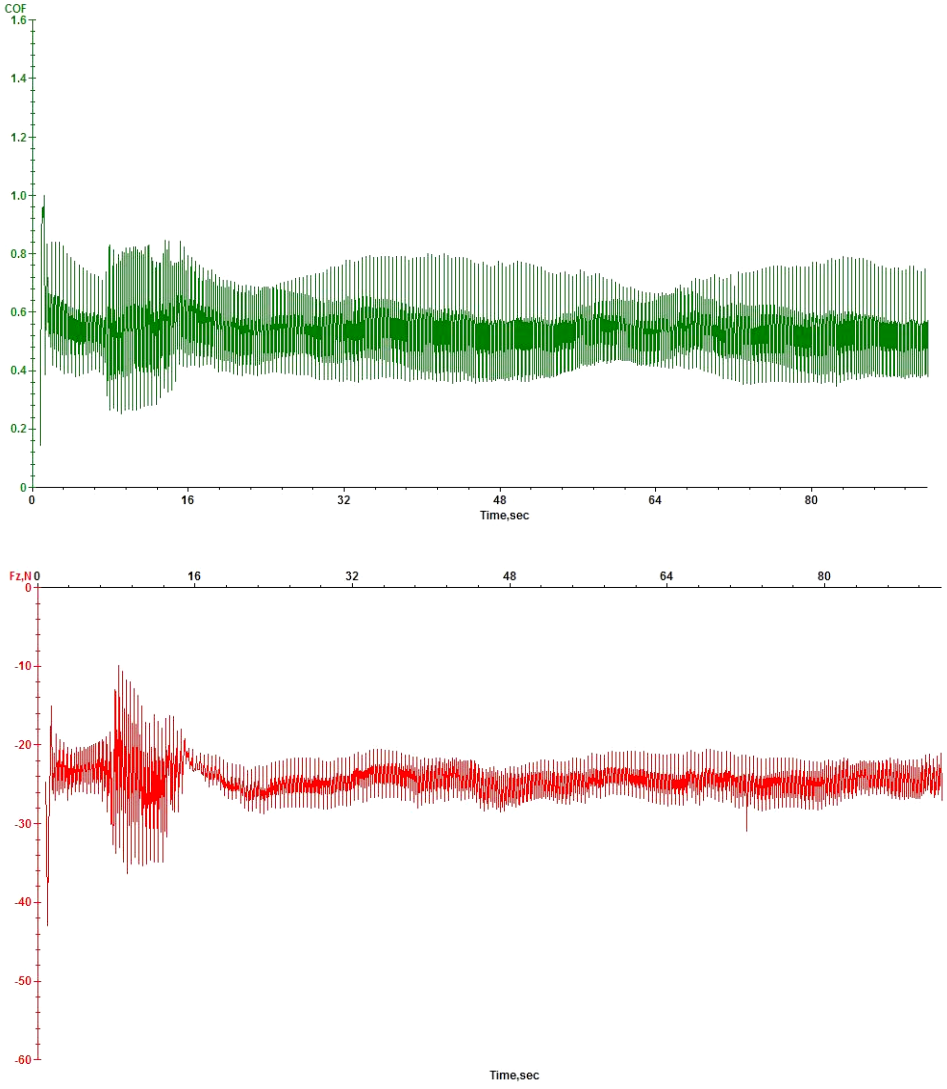

Figure 3.18. The coefficient of friction (top) and normal force (bottom) versus time for the uncoated ceramic tile

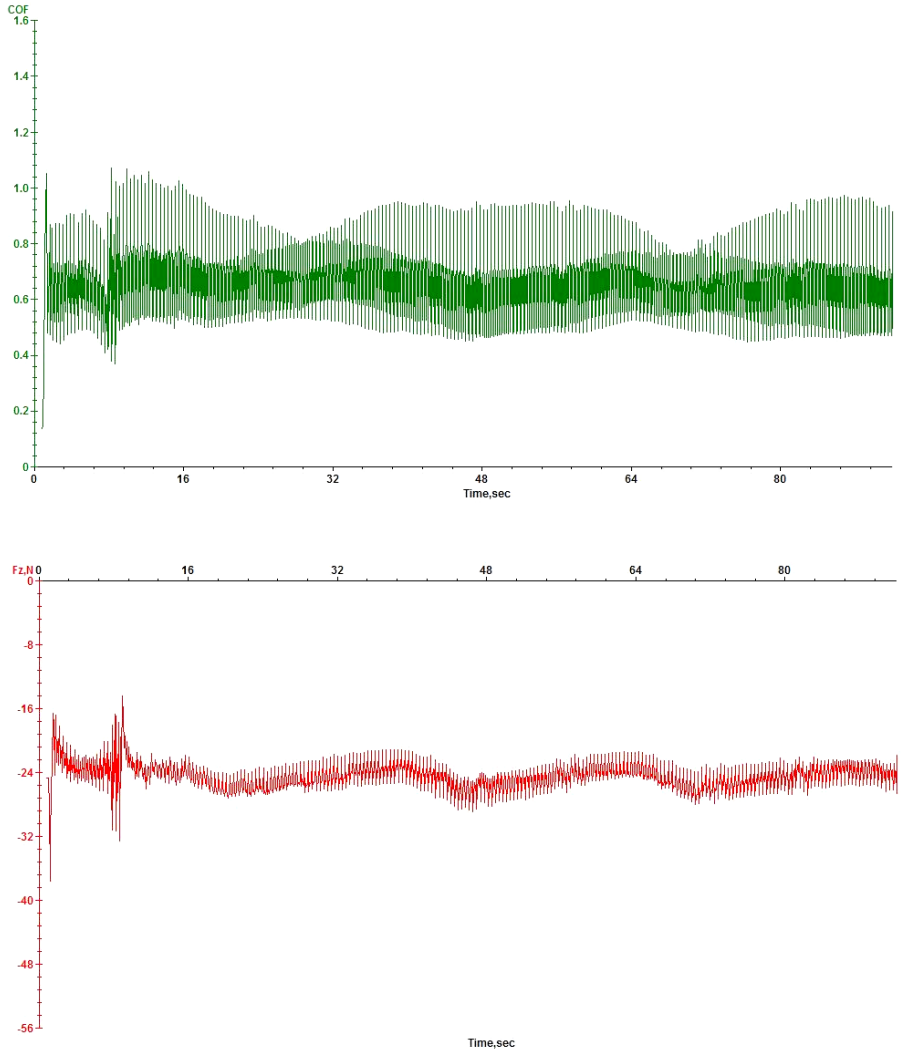

Figure 3.19. The coefficient of friction (top) and normal force (bottom) versus time for the sample R2

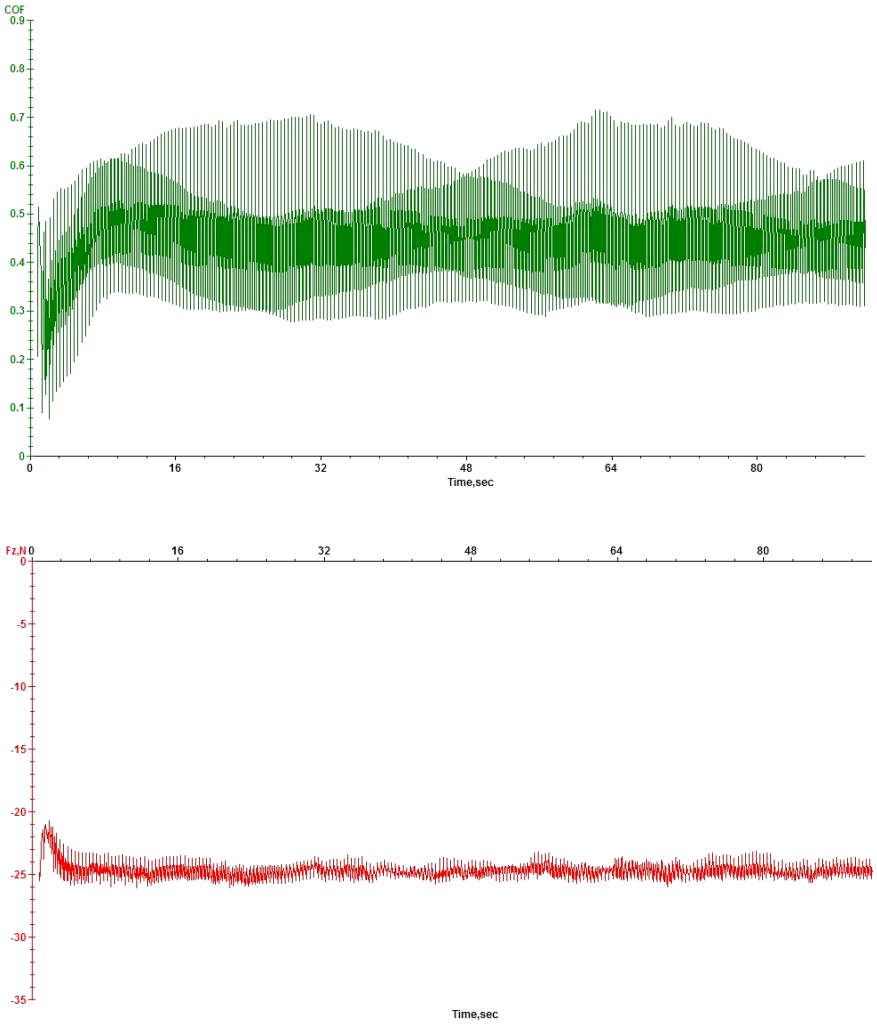

Figure 3.20. The coefficient of friction (top) and normal force (bottom) versus time for the sample R5

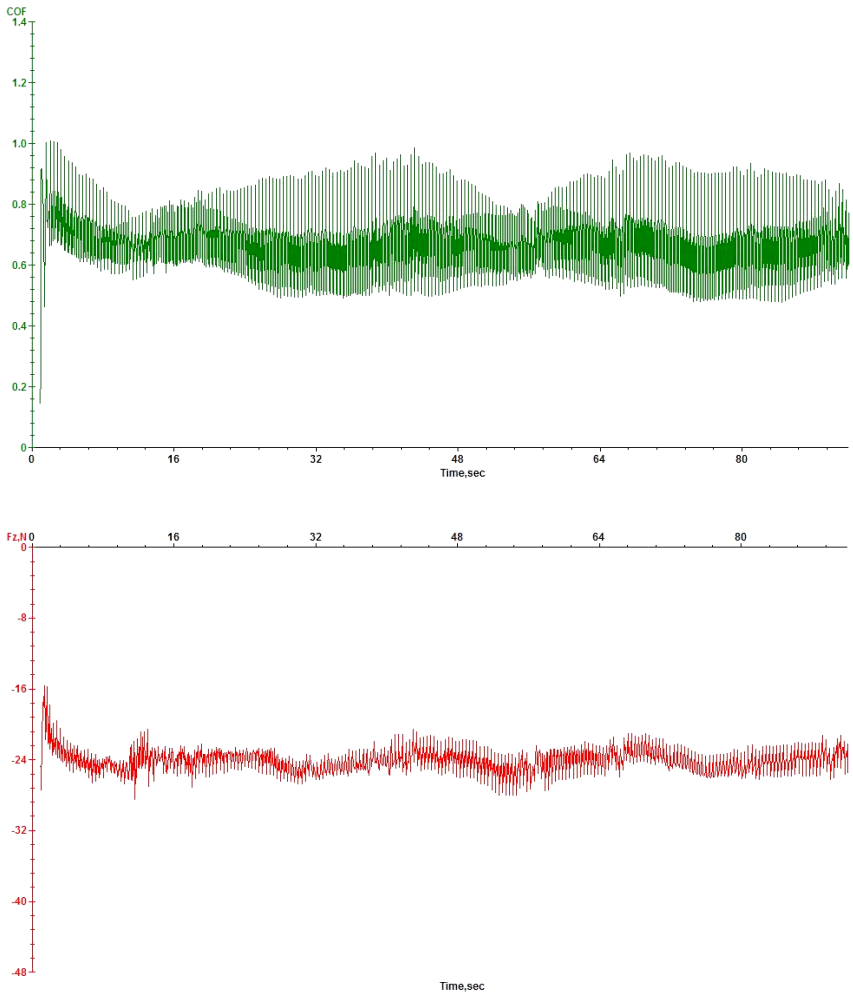

Figure 3.21. The coefficient of friction (top) and normal force (bottom) versus time for the sample R7

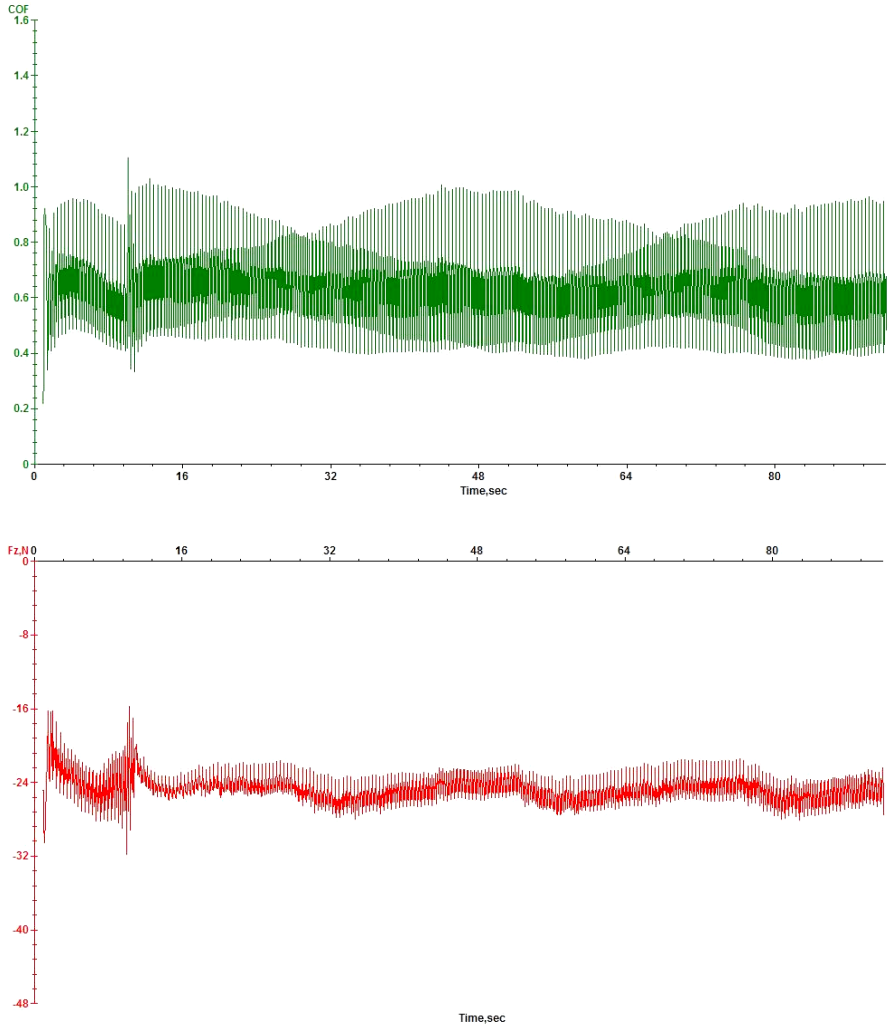

Figure 3.22. The coefficient of friction (top) and normal force (bottom) versus time for the sample R9

Figures 3.19-3.22 report on the values of the applied load (F_z) and coefficient of friction (COF) versus time for tested coatings. Table 3.5 summarizes the average COF's for samples R2, R5, R7, and R9. Higher coefficient of friction indicates better abrasion resistance and that the coating is not being erased from the surface of the tile during the tribological test. The industry standards set by Underwriters Laboratory (UL) reported the average coefficients of friction for the ceramic tiles from 0.3 to 0.6. The tribological tests provided the average coefficient of friction (F_x/F_z) of 0.45 for uncoated reference ceramic tiles, which is close to standard values. The average COF for the coated samples is 0.61, even higher than the result for the uncoated tile, possibly by enhanced roughness. The coated tiles R5 had COF which is similar to uncoated tiles due to using very high dilution rate and higher dosage of TiO_2 which to a high extent remained unconnected to the surface layer. Since the applied coatings did not reduce the abrasion resistance of ceramic tiles, it can be concluded that the developed coatings have a solid structure, and are not erased by the rubber.

Table 3.5. Coefficients of friction for samples R2-R9

№ of Sample	Coefficient of friction
R2	0.6615
R5	0.4496
R7	0.6741
R9	0.6323

All tested samples R2, R7, R9 demonstrated approximately equal coefficients of friction (Figures 3.19-3.22). To accurately evaluate the effect of tribological tests on the performance of the coatings, tested tiles were examined under the confocal microscope. Figure 3.23 represents the CLSM images of samples R2, R5, R7, R9, with 20X magnification after testing on the tribometer. Since the rubber particles remain on the surface of the coating, the coating had a stronger structure than the rubber and was not

erased from the surface. White particles under the rubber are the components of the coating that remained on the surface. The results of conducted tribological tests demonstrated that the investigated coatings have good abrasion resistance and adhesion to the substrate, and, therefore, will potentially demonstrate good durability.

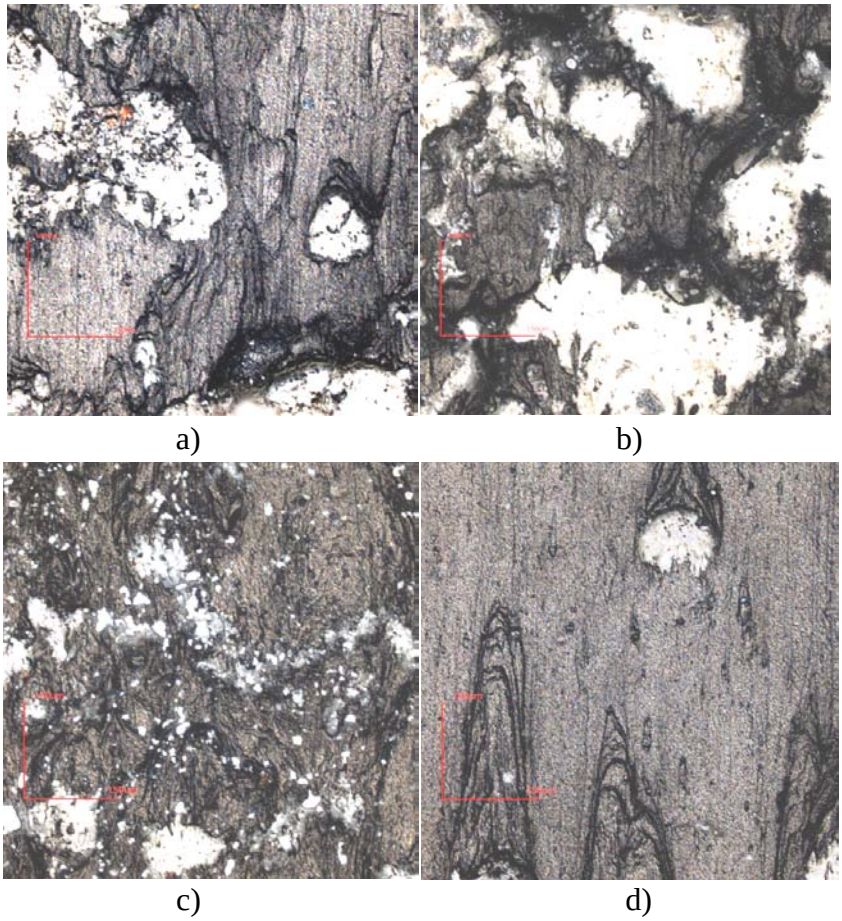

Figure 3.23. The surface of the coating observed after tribological test under the confocal microscope with 20X magnification for samples R2 (a), R5 (b), R7 (c), and R9 (d)

4. The Optimization of the Composition and Implementation of TiO_2 Coatings

Since several compositions of the coatings were developed and tested, and their properties were investigated, the optimized coating can be created based on the analysis of the tests results on photocatalytic properties, abrasion resistance, and the damage assessment observed under confocal microscope. For an effective application, the optimized coating should be as thin as possible to ensure the photocatalytic reaction and prevent the crack formation. The amount of the titanium dioxide should be minimized, meanwhile preserving the photocatalytic degradation at up to 40 %. The abrasion resistance and the adhesion to the ceramic tiles were found to be appropriate for the investigated coating materials. Therefore, the thinner layer of the coating was assumed to have a good adhesion and the abrasion resistance.

Taking into the consideration all the required characteristics of the optimal coating, the new final composition was developed. The final coating formulation contained 2.1 % of TiO_2, 4.1 % of H_3PO_4, and 93.8 % of water (by weight). This coating is more diluted than previously investigated samples, and the TiO_2/H_3PO_4 ratio was reduced to minimize the usage of the titanium dioxide and prevent the distribution of multiple TiO_2 layers on the surface of the coating.

The coating was applied on the ceramic tile, exposed to the thermal treatment in the furnace at 250 ˚C during 1 hour, and tested for photocatalytic properties, abrasion resistance, and also observed under scanning electron and confocal microscopes.

4.1. The photocatalytic properties of the coating

The optimal coating was tested on NO-NO_x analyzer for the photocatalytic properties. All initial experimental conditions, such as the intensity of the UV irradiation, humidity in the chamber, the initial preset NO_x concentration, and the surface area of the tile covered with the coating, remained the same as in the previous experiments for the samples R1-R8. Figure 4.1 illustrates the NO_x decomposition for the optimal coating by recording the concentrations of NO and NO_x versus time for the initial concentrations of NO_x of 2.7 ppm and 1.5 ppm.

The results of the photocatalytic experiments prove that even extremely diluted coating with minimized amounts of the titanium dioxide provides the significant reduction of NO_x concentration of up to 15 % ppm and up to 35 % at the initial NO_x concentration of 2.7 ppm and 1.5 ppm, respectively. The results demonstrate that the developed coating has effective photocatalytic properties required for the reduction of NO and NOx.

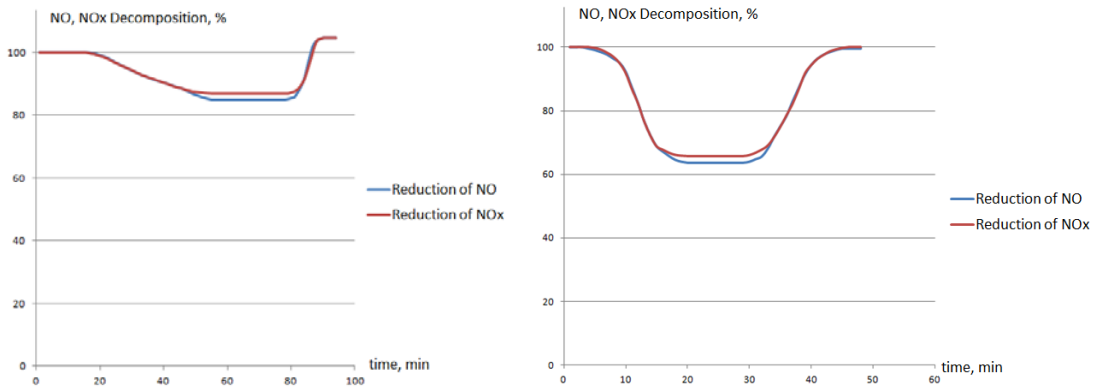

Figure 4.1. NO_x decomposition for the optimal coating at the NO_x concentration of 2.7 ppm (left) and 1.5 ppm (right)

4.2. The results of tests on the crack formation

The surface of the coating was observed under the confocal microscope to investigate the structure and possible crack formation. Figure 4.2 provides the images of the surface of the coating observed under CLSM with 20X magnification.

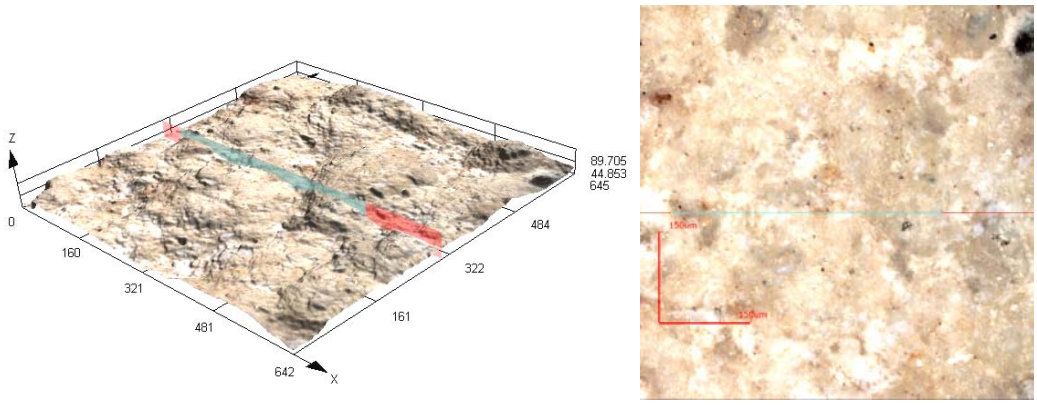

Figure 4.2. The TiO_2-phosphate coating applied on the ceramic tile observed under a confocal microscope with 20X magnification

White particles of TiO_2 and titanium phosphates are seen on the surface of ceramic tile, which is illustrated in Figure 4.2. There are no cracks on the surface of the coating. The coating is very thin and appears to be applied evenly on the surface of the tile, which allows avoiding the crack formation, even if the coating is exposed to the thermal treatment. The absence of cracks contributes to better adhesion to the surface of the tile and better abrasion resistance, because there is no risk of the exfoliation due to the shrinkage of the thicker layers of the coating.

4.3. The abrasion resistance of the coating

The developed TiO_2-phosphate coating was tested using the tribometer. The COF of 0.66 was obtained, which is similar to the average coefficient of friction for the samples R2 and R7. It can be concluded that the optimal coating has a good abrasion resistance and adhesion to the surface of the tile. Figure 4.3 illustrates the coefficient of

friction and normal force versus time for the optimal sample. The data from CLSM, represented in Figure 4.4, confirm that the coating is not erased from the surface during the tribological tests, and, therefore, will potentially demonstrate a good durability.

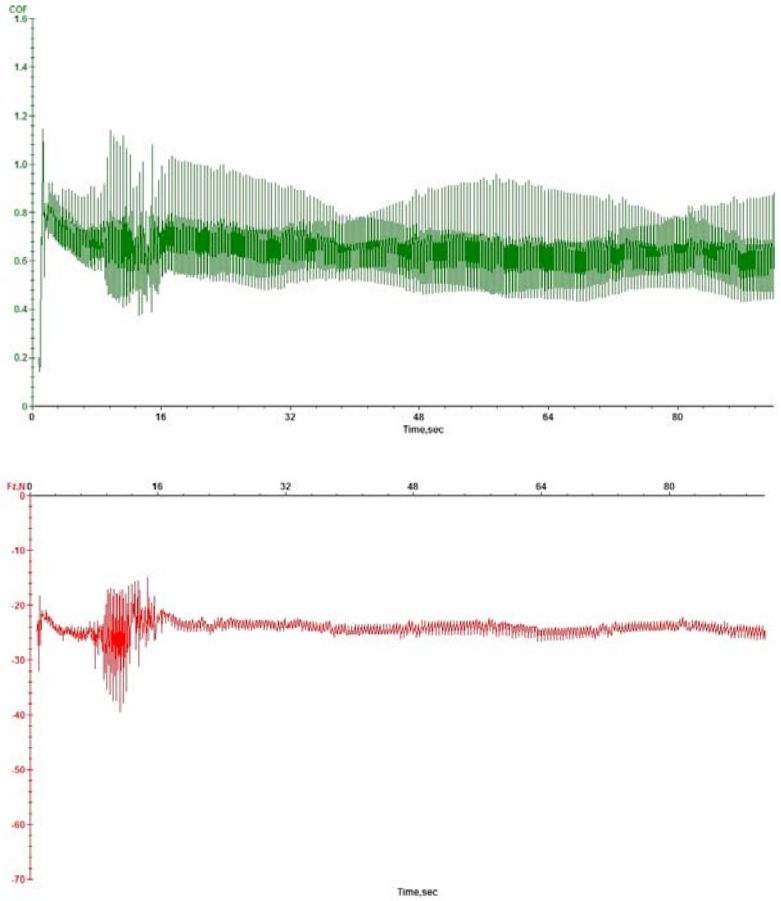

Figure 4.3. The coefficient of friction (top) and normal force (bottom) versus time for the optimal sample

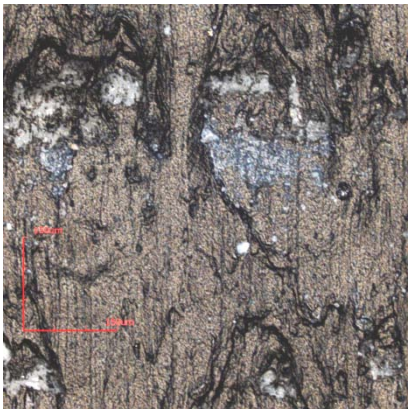

Figure 4.4. The surface of the optimal coating observed after tribological test under the confocal microscope with 20X magnification

4.4. The hydrophobization of the coating

The TiO_2-phosphate-based coating itself is hydrophilic. To make it hydrophobic, the water-based siloxane emulsion was applied on the surface of the coating. After 24 hours from the application, the siloxane emulsion attained the hydrophobic properties and the tiles covered with two-layer coating were tested for the contact angle. The contact angle was measured three times, and the images of droplets of water on the surface of the coating, obtained in three tests, are introduced in Figure 4.5. The resulting average CA was 114˚.

Since the $CA > 90^{\circ}$, the developed coating is hydrophobic ($90^{\circ} < CA < 120^{\circ}$), however, it was important to investigate how the water-based siloxane emulsion influenced the abrasion resistance and photocatalytic properties of the coating.

Figure 4.5. The CA for developed hydrophobic coating

The elemental composition of the developed coating was observed under a scanning electron microscope (SEM) to observe the uniformity of coating, and analyze

the chemical composition of the coating. Three samples were tested on SEM. The first sample is the uncoated reference ceramic tile. The second sample is the tile covered with the one-layer titanium phosphate coating, and the third one is the ceramic tile covered with the two-layer hydrophobic coating.

Figure 4.6 reports on the image of the uncoated ceramic tile, taken with 1,500x magnification. Figure 4.7 illustrates the images of the ceramic tile covered with the one-layer titanium phosphate coating (and not covered with the siloxane emulsion), taken under SEM with 5,500x and 5,000x magnifications. In comparison with the SEM images of the uncoated ceramic tile, it can be observed in Figure 4.7 that the titanium phosphates evenly cover the surface of the ceramic tile and are well attached to the surface.

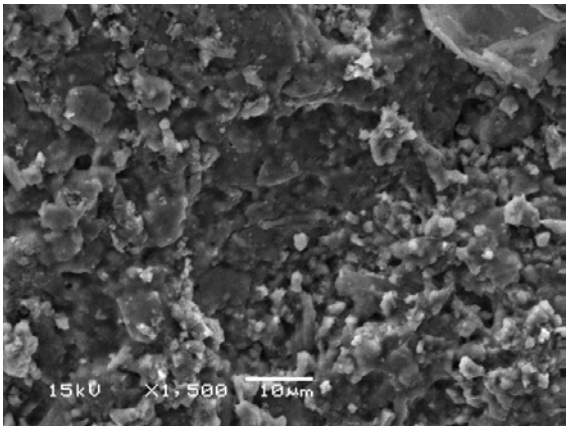

Figure 4.6. The ceramic tile surface observed under scanning electron microscope with 1,500x magnification

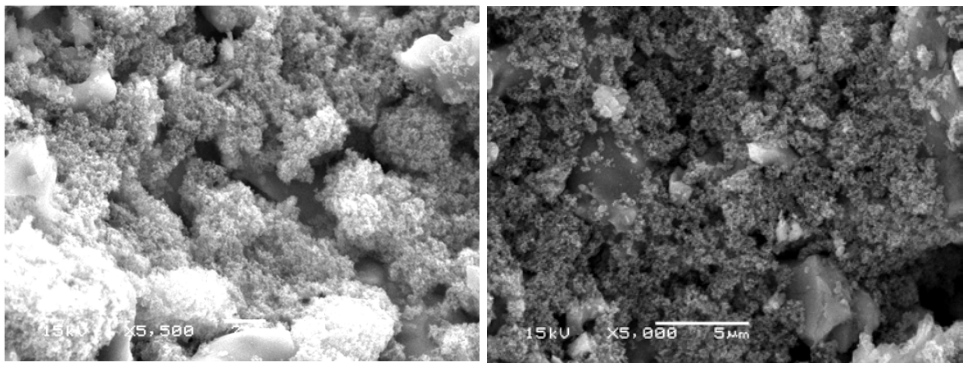

Figure 4.7. Optimal titanium phosphate coating without hydrophobic coating applied on the ceramic tile observed under SEM with 5,500x (left) and 5,000x (right) magnification

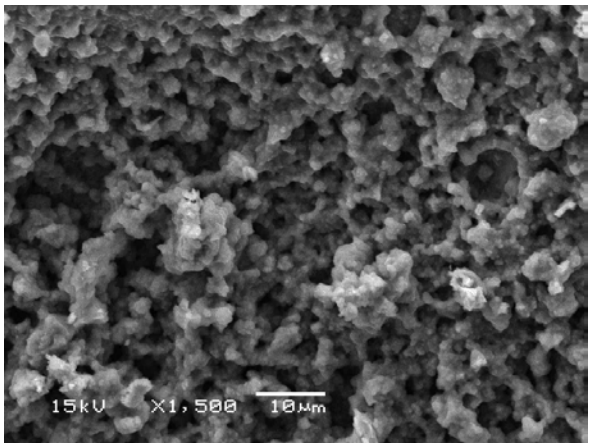

Figure 4.8. The titanium phosphate coating covered with the hydrophobic coating applied on the ceramic tile observed under SEM with 1,500x magnification

Figure 4.8 illustrates the ceramic tile covered with the two-layer hydrophobic coating, observed under SEM at 1,500X magnification. It can be seen that the structure of ceramic tile surface covered with two-layer hydrophobic coating differs from the surface structure of the uncoated ceramic tile and ceramic tile covered with the one-layer titanium phosphate coating. With hydrophobic coating, the titanium phosphates are not seen as clearly, but the surface structure is clear and uniform.

The elemental analysis of uncoated reference tile and coated ceramic tile was conducted on the scanning electron microscope. Figure 4.9 reports on the elemental compositions of uncoated ceramic tile. The analysis of the elemental composition for the tile coated with one-layer titanium phosphate coating is introduced in Figure 4.10.

Figure 4.11 provides the elemental analysis of the ceramic tile, coated with a two-layer hydrophobic coating. The percentages of chemical elements, which can be found in the coated tiles, are illustrated in Tables 4.1-4.3. Table 4.1 illustrates the percentage of chemical elements on the surface of the reference tile. Table 4.2 illustrates the percentage of chemical elements distribution for the tile covered with the hydrophilic (one-layer) coating. Table 4.3 reports on the elemental analysis of chemical elements for the tile covered with the hydrophilic titanium phosphate coating and siloxane emulsion.

The main elements, typical for clay, such as silicon, oxygen, carbon, magnesium, potassium, calcium and aluminum are introduced in the elemental composition of the ceramic tile. In comparison with the elemental composition of the uncoated tile, the tiles covered with the one-layer titanium phosphate coating and two-layer hydrophobic coating contain some additional elements, such as titanium and phosphorous. It can be observed that different spectra contain different amounts of elements, for example, the amounts of titanium by weight is two times higher in the spectrum 2 than in the spectrum 1 for the tile covered with the titanium phosphate coating and not covered with siloxane emulsion. However, the elemental composition for the tile coated with the hydrophobic two-layer coating is similar to the chemical composition of the tile covered with a one-layer hydrophilic coating, as hydrophobic emulsion is not changing the chemical build up of the coating.

In general, the structures and elemental compositions are similar for each spectrum of the investigated samples. This means that the coating has even structure, which is observed in the SEM images (Figures 4.6-4.8). TiO_2-phosphate particles are extremely thin, adhered and evenly distributed on the surface of the tile, which is a required characteristic of the coating.

Table 4.1. Elemental composition of the reference tile

Element	Spectrum 1		Element	Spectrum 2	
	Weight %	Atomic %		Weight %	Atomic %
O	47.73	54.50	O	47.35	59.10
Si	20.76	13.50	Si	22.16	15.75
Na	0.37	0.29	Na	0.16	0.14
Mg	8.16	6.13	Mg	6.21	5.10
Al	5.53	3.74	Al	12.89	9.54
K	0.28	0.13	K	0.73	0.37
Ca	4.15	1.89	Ca	6.32	3.15
C	13.02	19.81	C	4.10	6.81
			Mn	0.09	0.03
Totals	100.00		Totals	100.00	

Table 4.2. Elemental composition of the tile covered with the hydrophilic coating

Element	Spectrum 1		Element	Spectrum 2	
	Weight %	Atomic %		Weight %	Atomic %
O	43.74	59.31	O	40.11	57.36
Na	0.22	0.21	Na	0.61	0.61
Mg	3.42	3.05	Mg	4.52	4.26
Al	13.71	11.02	Al	6.43	5.45
Si	26.61	20.55	Si	25.99	21.17
P	0.28	0.20	P	0.39	0.29
K	1.03	0.57	K	0.64	0.37
Ca	2.84	1.53	Ca	3.34	1.90
Ti	8.72	3.95	Ti	17.98	8.59
Totals	100.00		Totals	100.00	

Table 4.3. Elemental composition of the tile covered with the hydrophobic coating

Element	Spectrum 1		Element	Spectrum 2	
	Weight %	Atomic %		Weight %	Atomic %
O	43.42	52.31	O	41.72	46.39
Ca	0.29	0.14	Na	0.12	0.09
Mg	2.00	1.59	Mg	0.25	0.18
Al	0.38	0.27	Al	0.04	0.03
Si	26.73	18.35	Si	21.68	13.73
P	0.56	0.35	P	0.43	0.25
Ti	13.91	5.60	Ti	13.00	4.83
K	0.09	0.04			
C	13.74	22.05			
Totals	100.00		Totals	100.00	

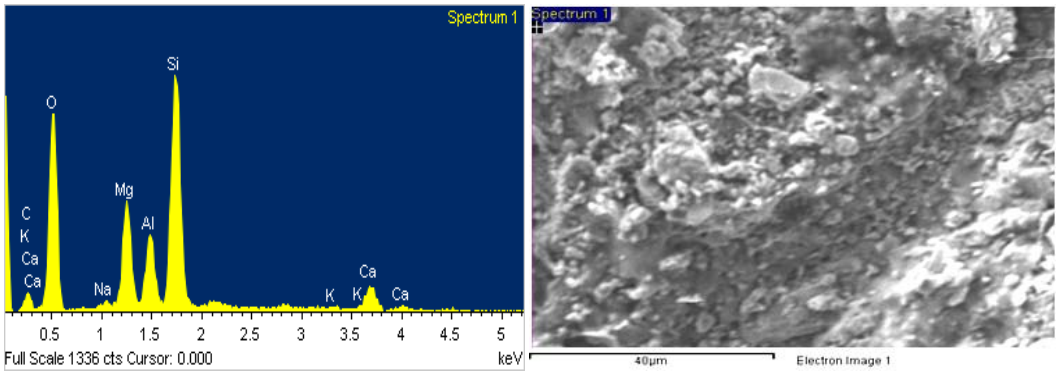

Spectrum 1

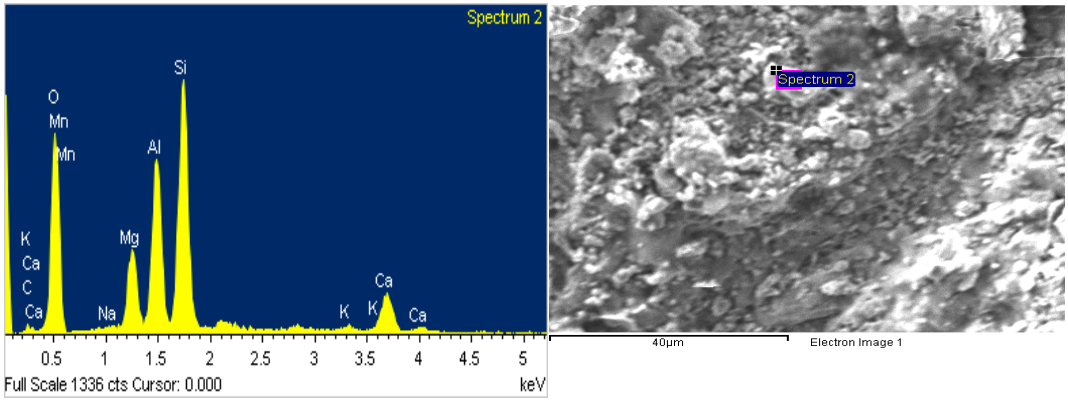

Spectrum 2

Figure 4.9. The elemental analysis of the uncoated ceramic tile

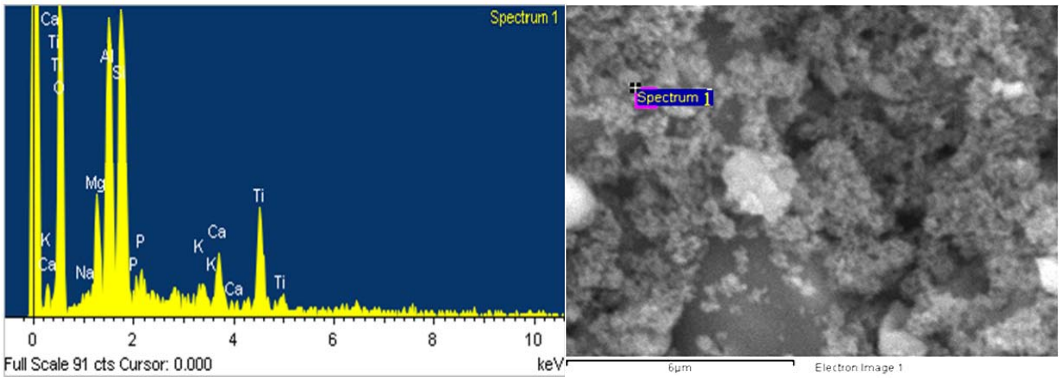

Spectrum 1

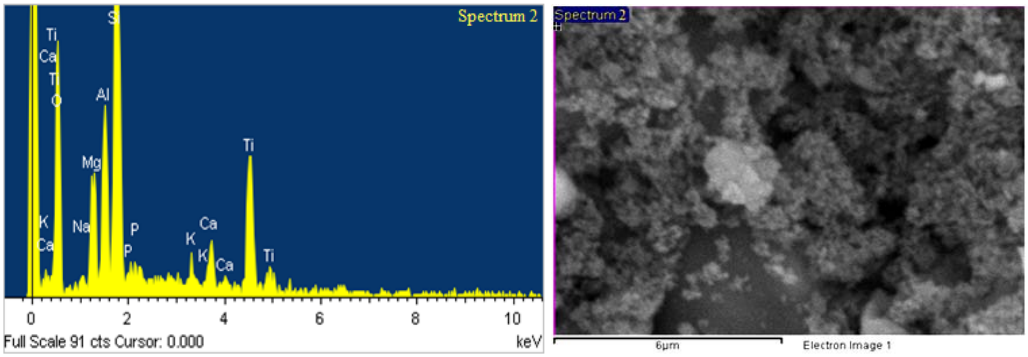

Spectrum 2

Figure 4.10. The elemental analysis of the ceramic tile covered with titanium phosphate coating

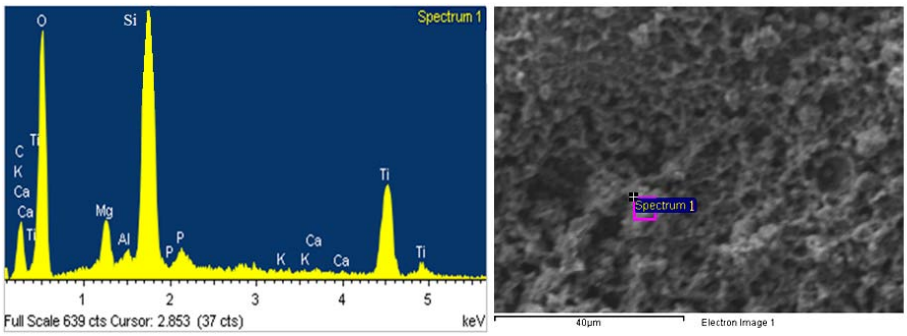

Spectrum 1

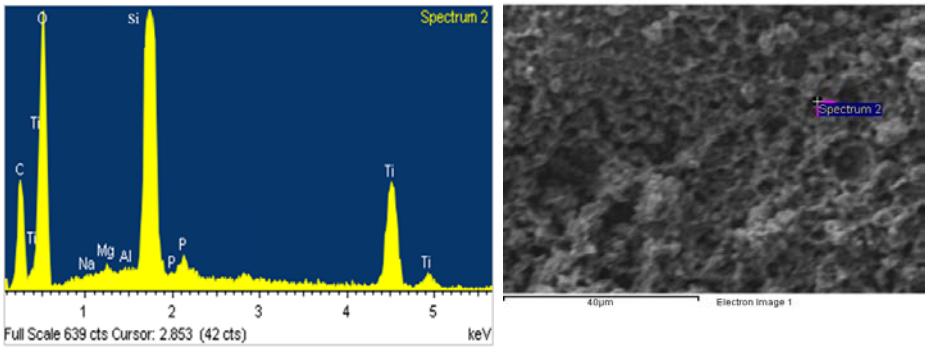

Spectrum 2

Figure 4.11. The elemental analysis of the ceramic tile covered with titanium phosphate coating and siloxane emulsion

4.5. The photocatalytic properties of developed coatings

Since the use of siloxane emulsion may reduce the decomposition rates of NO_x, a new test with the tile covered with two-layer hydrophobic coating was conducted on the NO-NO_x analyzer. The results of the tests are introduced in Figure 4.12.

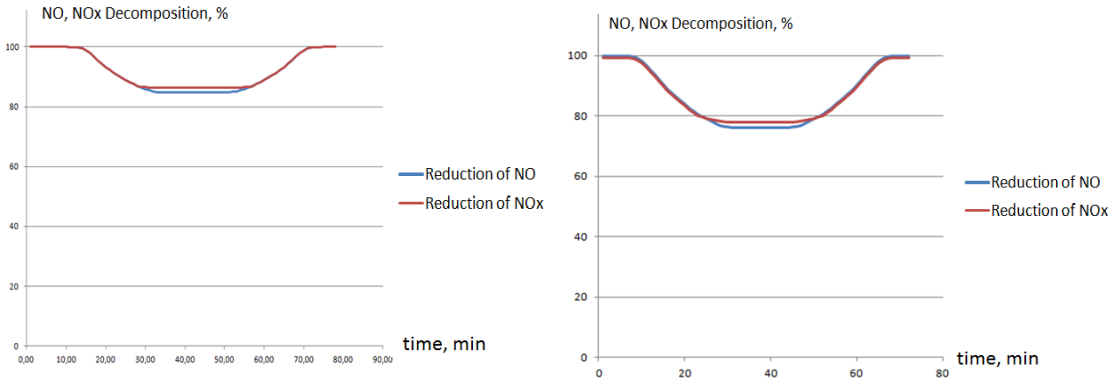

Figure 4.12. NO_x decomposition for the hydrophobic coating at the NO_x concentration of 2.7 ppm (left) and 1.5 ppm (right)

The concentration of NO_x gas was decreased by 23 %, which is less than the results for the untreated coating (35 %), but the decomposition of NO_x is still significant, despite the presence of the hydrophobic coating. The results of the photocatalytic experiment proved that it is possible to combine self-cleaning and hydrophobic properties in a composite coating, which is the important outcome of this research.

4.6. The abrasion resistance of developed coatings

The resulting hydrophobic coating was tested on the tribometer. The normal force and resulting coefficient of friction are introduced in Figure 4.13. The COF was slightly reduced after the hydrophobization of the coating to the level of 0.55 but remains higher than the COF obtained for the uncoated tile, demonstrating an excellent improvement for dry traction of tires. Figure 4.14 represents the results from CLSM for the hydrophobic coating.

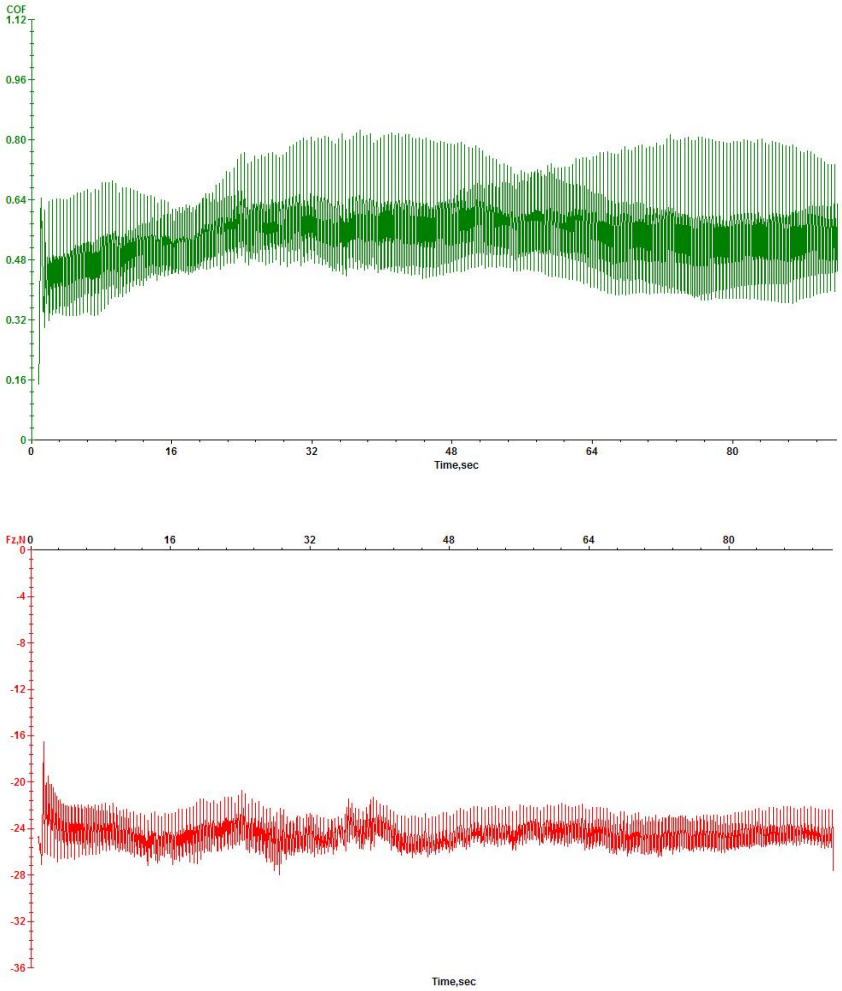

Figure 4.13. The coefficient of friction (top) and normal force (bottom) versus time for the hydrophobic sample

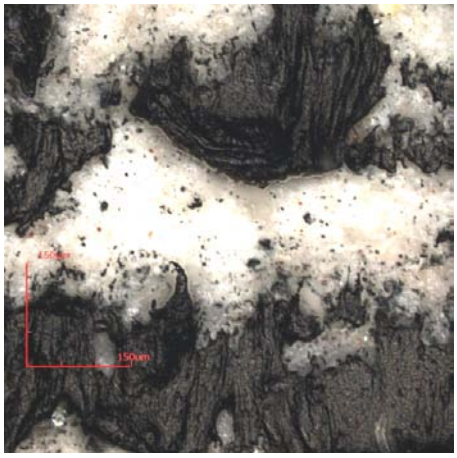

Figure 4.14. The surface of the optimal hydrophobic coating observed after the tribological test under the confocal microscope with 20X magnification

5. Conclusions

Civil engineers have used the titanium dioxide component capable of cleaning the air from harmful pollutants for the facades, roads and other structures. Portland cement based compositions were mostly used to adhere the active components to the surface of the structure. Such an application requires the use of relatively large amounts of TiO_2. Alternatively, the use of TiO_2 not bonded with coatings leads to relatively easy removal and associated health issues. A new two stage coating concept allows creating the extremely thin titanium phosphate-based coating characterized by minimal consumption of TiO_2 and good photocatalytic activity and, upon hydrophobization treatment, possesses hydrophobic properties.

Since one of the most important parameters for the coating is durability, the developed composition was based on the titanium phosphates, the solid materials with high compressive strength reaching up to 61.5 MPa.

It was found that all tested samples have a good adhesion to the surface of the tile and developed coatings are not removed from the surface during the tribological tests. However, it was realized that the thickness of the coating should be significantly reduced to avoid the formation of cracks. It was realized that extremely diluted compositions resulted in the almost invisible thin coatings, which evenly covered the tiles without cracks on the surface.

Preliminary results demonstrated that increasing of the TiO_2 amounts in comparison with the stoichiometric proportion leads to the significant improvement of photocatalytic properties up to 97 % of NO_x decomposition (at the initial NO_x concentration of 1.5 ppm). Since the objective of this research was to minimize the titanium dioxide, while maintaining the 30-40 % of NO_x decomposition, the optimized

coating was selected with a TiO_2/H_3PO_4 ratio close to the stoichiometric (36/64 by weight).

The conducted research proved that the coating attained the hydrophobic properties and at the same time did not lose the photocatalytic and mechanical properties.

The research was conducted on the effect of magnesium oxide on the formation of phosphates and the potential for reduction of temperature required for the formation of the titanium phosphates. Since the magnesium phosphates harden at room temperature, and titanium phosphates require 250 ˚C for the complete hardening, MgO was intended to help to reduce the temperature of the thermal treatment. However, phosphates were formed very fast, and the magnesium oxide played the role of the passivator, therefore, the expected performance of the coating was not achieved. As a result, the magnesium oxide was not recommended as a component of the optimized coating.

The developed coating applied on the surface of the tile was investigated under the SEM. It was observed that the phosphates and siloxane emulsion are evenly applied and properly adhered to the surface of the tile. These conclusions were confirmed by the elemental analysis, which demonstrated that all investigated spectra have similar elemental compositions.

Future Work

The reported research has demonstrated that the titanium phosphate - based coatings have a good photocatalytic performance and excellent abrasion resistance. However, the application of the coating requires the thermal treatment. In this research, the coatings hardened in the muffle furnace, and it would be beneficial to optimize the application and curing procedure. Future work would also include the improvement of the photocatalytic and hydrophobic properties, further minimizing the titanium dioxide consumption.

References

1. Abdel Rahman, R.O., Rakhimov, R.Z., Rakhimova, N.R., Ojovan, M.I. (2014). "Cementitious materials for nuclear waste immobilization." WILEY: 1-248.

2. Aziz, H.A., Umar, M. (2013). "Photocatalytic degradation of organic pollutants in water." INTECH: Chapter 8.

3. Batrakov, V. (1998). "Modified concrete. Theory and practice." The 2nd Edition revised and expanded: 51-54.

4. Beeldens, A. (2016). "An environmentally friendly solution for air purification and self- cleaning effect: the application of TiO_2 as a photocatalyst in concrete." Transp. R.A. Eur.

5. Bentz, D.P., Ferraris, C.F., Jones, S.Z., Lootens, D., and Zunino, F. (2017)."Limestone and silica powder replacements for cement: Early-age performance." Cement and Concrete Composites: 78, 43-56.

6. Binas, V., Venieri, D., Kotzias D., and Kiriakidis, G. (2017). "Modified TiO_2 based photocatalysts for improved air and health quality." Journal of Materiomics: 6-7.

7. Birgisson, B., Mukhopadhyay, A.K., Geary, G., Khan, M., Sobolev, K. (2012). "Nanotechnology in concrete materials. A Synopsis." Transportation Research Board: 12-28.

8. Bittnar, Z., Bartos, P.J.M., Nemecek, J., Smilauer, V., Zeman, J. (2009). "Nanotechnology in construction: proceedings of the NICOM3." Springer.

9. Colmenares, J. C., Luque, R., Campelo, J. M., Colmenares, F., Karpiński, Z., Angel Romero, A. (2009)."Nanostructured photocatalysts and their applications in the photocatalytic transformation of lignocellulosic biomass: An Overview." Materials 2009: 2228-2258.

10. Crain, N., Juenger, M., Cros, C., Terpeluk, A. (2017). "Laboratory and field studies of photocatalytic NOx and O3 removal by coatings on concrete." The University of Texas at Austin. Center for Transportation Research: 1-345.

11. Das, I.; Mishra, M. K; Medda, S.K; De, G. (2014). "Durable superhydrophobic ZnO–SiO_2 films: a new approach to enhance the abrasion resistant property of trimethylsilyl functionalized SiO_2 nanoparticles on glass." RSC Advances: 54989–54997.

12. Engel, A., Große, J., Dillert, R., Bahnemann, Detlef W. (2016). "The influence of irradiance and humidity on the photocatalytic conversion of nitrogen(II) oxide." Journal of Advanced Oxidation Technologies: 195-203.

13. Faraldos, M., Kropp, R., Anderson, M., Sobolev, K. (2015). "Photocatalytic hydrophobic concrete coatings to combat air pollution." Catalysis Today: 228-236.

14. Fedorov, N. F., Sychev, M.M., Sudakas, L.I. (1974). "Hardening of binders." Stroyizdat.: 80.

15. Flores-Vivian, I., Hejazi, V., Kozhukhova, M.I., Nosonovsky, M., and Sobolev, K. (2013). "Self-assembling particle-siloxane coatings for superhydrophobic concrete." ACS Applied Materials & Interfaces: 13284–13294.

16. Hanaor, D.A.H.; Sorrell, C. (2011). "Review of the anatase to rutile phase transformation." Journal of Materials Science: 855–874.

17. Hu, Z.; Zen, X.; Gong, J.; Deng, Y. (2009). "Water resistance improvement of paper by superhydrophobic modification with microsized $CaCO_3$ and fatty acid coating." Colloids and Surfaces A: Physicochemical and Engineering Aspects.

18. Kenneth, B. (2015). "Coating deterioration." ASM International, Protective Organic Coatings: 462-472.

19. Khan, S.U., Nuruddin, M.F., Ayub, T., and Shafiq, N. (2014). "Effects of different mineral admixtures on the properties of fresh concrete." Scientific World Journal: 11.

20. Kumar, A. and Pandey, G. (2017). "A review on the factors affecting the photocatalytic degradation of hazardous materials." International Journal of Materials Science and Engineering:106–114.

21. Kumar, S.A., Narayanan S. (2002). "Thermal properties siliconized interpenetrating epoxy coatings." Progress in Organic Coatings: 323-330.

22. Lin, J.; Chen, H.; Fei, T.; Zhang, J. (2013). "Highly transparent superhydrophobic organic-inorganic nanocoating from the aggregation of silica nanoparticles."

23. Mahlambi, M. M., Ngila, C.J., and Mamba, B.B. (2015). "Recent developments in environmental photocatalytic degradation of organic pollutants: the case of titanium dioxide nanoparticles—A review." Journal of Nanomaterials: 1-29.

24. Pawley, J.B. (editor) (2006). "Handbook of Biological Confocal Microscopy (3rd ed.)." Berlin: Springer.

25. Pole, G.R., Beinlich Jr., A.W., Gilbert, N. (1946). "Physical properties of some high-temperature refractory compositions." American Ceramic Society: 208-228.

26. Ranjit, K., Odedra, K., Parmar, A., Arora, N. (2014). "Photocatalytic self-cleaning concrete." International Journal for Scientific Research & Development: 2521-2523.

27. Rostami, N. (2014). "Development of novel magnesium phosphate bone cement University of Toledo." University of Toledo.

28. Shang, H.M. (2005). "Optically transparent superhydrophobic silica-based films." Thin Solid Films: 37-43.

29. Srimaneepong, V., Kosaiyakanon, Y., and Sriyudthsak, M. (2016). "Electrical resistance of dental luting cements investigated by the impedance methodology related to their porosities and solubility." 10th World Biomaterials Congress, Montréal, Canada.

30. Striley, C. (2011). "Current Intelligence Bulletin 63: Occupational exposure to titanium dioxide." U.S. National Institute for Occupational Safety and Health: 160-161.

31. Topličić-Ćurčić, G., Jevtić, D., Grdić, D., Ristić, N., Grdić, Z. (2017). "Photocatalytic concrete – environment-friendly material." 5th International Conference. Contemporary achievements in civil engineering 21.

32. Van Driel, B.A., Kooyman, P., Van den Berg, K., Schmidt-Ott, A., Dik, J. (2016). "A quick assessment of the photocatalytic activity of TiO_2 pigments — From lab to conservation studio!" Microchemical Journal: 162-171.

33. Wang, J., Yu, J., Zhu, X., Kong, X. (2012). "Preparation of hollow TiO_2 nanoparticles through TiO_2 deposition on polystyrene latex particles and characterizations of their structure and photocatalytic activity." Nanoscale Research Letters: 646-647.

34. Wen, K., Liu, M., Liu, X., Deng, C., and Zhou, K. (2017). "Deposition of photocatalytic TiO_2 coating by modifying the solidification pathway in plasma spraying." Coatings 2017: 169.

35. Zhao, D., Chen, C., Wang, Y., Ji, H., Ma, W., Zang, L., and Zhao J. (2008)."Surface modification of TiO_2 by phosphate: effect on photocatalytic activity and mechanism implication." Journal of Physical Chemistry: 5993-6001.

36. http://www.differencebetween.net/science/chemistry-science/differences-between-rutile-and-anatase-titanium-dioxide

37. https://hisour.com/binder-material-21546

38. https://www.chinapowdercoating.com/super-hydrophobic-coatings-create

39. http://everything.explained.today/Tribometer

40. http://stroy-server.ru/notes/fosfatnye-tsementy